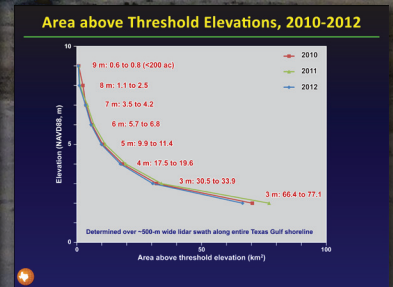
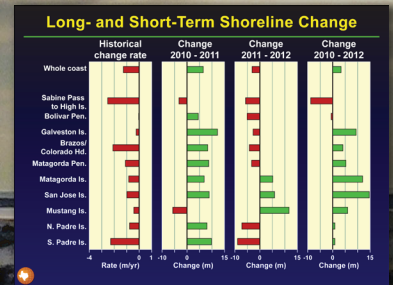
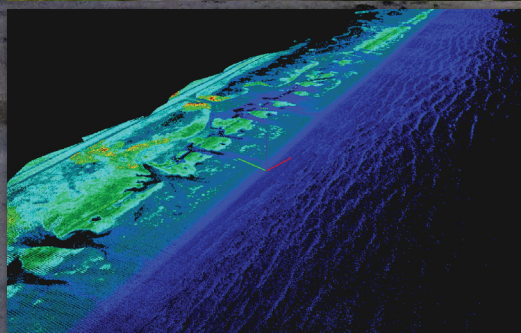


FINAL REPORT

Shoreline, Beach, and Dune Morphodynamics, Texas Gulf Coast

Jeffrey G. Paine, Tiffany Caudle, and John Andrews



Bureau of Economic Geology

Scott W. Tinker, Director

Jackson School of Geosciences, The University of Texas at Austin, Austin, Texas 78713-8924



JACKSON
SCHOOL OF GEOSCIENCES

Final Report Prepared for
General Land Office under
Contract No. 09-242-000-3789.

Page intentionally blank

SHORELINE, BEACH, AND DUNE MORPHODYNAMICS,
TEXAS GULF COAST

by

Jeffrey G. Paine, Tiffany Caudle, and John Andrews
Bureau of Economic Geology
John A. and Katherine G. Jackson School of Geosciences
The University of Texas at Austin
University Station, Box X
Austin, Texas 78713

with contributions from
James C. Gibeaut, Diana Del Angel, and Eleonor Taylor
Harte Research Institute for Gulf of Mexico Studies
Texas A&M University–Corpus Christi

Corresponding author
jeff.paine@beg.utexas.edu
(512) 471-1260

Final Report Prepared for the General Land Office under Contract No. 09-242-000-3789.

October 31, 2013



JACKSON
SCHOOL OF GEOSCIENCES

Page intentionally blank

CONTENTS

Abstract	v
Introduction	1
Relative Sea Level	4
Tropical Cyclones	8
Methods	10
Lidar Data Acquisition	10
Lidar Data Processing	15
Shoreline	19
Potential Vegetation Line	20
Landward Dune Boundary	21
Storm Susceptibility Index	22
Texas Gulf Shoreline Change	23
Short-term Shoreline Change, 2010 to 2012	25
Incremental Change between 2010 and 2011	25
Incremental Change between 2011 and 2012	29
Net Change between 2010 and 2012	32
Elevation-Threshold Areas	35
Upper Coast	39
Middle Coast	39
Lower Coast	41
Storm Susceptibility Index	44
Conclusions	46
Acknowledgments	47
References	47
Appendix A: Elevation-Threshold Areas	53
April 2010 Airborne Lidar Survey	53
April 2011 Airborne Lidar Survey	54
February 2012 Airborne Lidar Survey	55

Appendix B: SBEACH Modeling	57
SBEACH Calibration	57
SBEACH Modeling	58
Representative Profiles.....	58
Synthetic Storms	59
Level of Protection Provided by Dune and Beach Environments	60
Appendix C: Data Volume Contents	63

FIGURES

1. Map of the Texas coastal zone	2
2. Sea-level trend at selected Texas tide gauges through 2012	6
3. Sea-level trend at Galveston Pier 21, 1908 to 2013.....	7
4. Coverage map of the 2010 lidar survey.....	11
5. Coverage map of the 2011 lidar survey.....	13
6. Coverage map of the 2012 lidar survey.....	14
7. Net rates of long-term change for the Texas Gulf shoreline	24
8. Net shoreline change between April 2010 and April 2011	26
9. Comparison of incremental shoreline change measured between 2010 and 2012 with long-term shoreline change along the Texas Gulf shoreline	27
10. Net shoreline change between April 2011 and February 2012	30
11. Net shoreline change between April 2010 and February 2012	33
12. Total area above threshold elevations in 2010, 2011, and 2012	37
13. Normalized area above threshold elevations for upper, middle, and lower coast counties, Texas Gulf coast.....	38
14. Sea Rim State Park DEM and area slices at threshold elevations	40
15. Matagorda Island DEM and area slices at threshold elevations	42
16. South Padre Island DEM and area slices at threshold elevations	43
17. Storm Susceptibility Index protection levels for the Texas coast	45

TABLES

1. Long-term rates of relative sea-level rise at select Texas tide gauges through 2012.	6
2. Tropical cyclones affecting the Texas coast between 1990 and 2013	9
3. GPS base stations used during the 2010, 2011, and 2012 airborne lidar surveys	16
4. Bias corrections and standard deviations for the 2010, 2011, and 2012 airborne lidar surveys.	18
5. Net shoreline change, April 2010 to April 2011	28
6. Net shoreline change, April 2011 to February 2012	31
7. Net shoreline change, April 2010 to February 2012	34
8. Eight protection levels of the Storm Susceptibility Index	44
B1. Synthetic storm parameters	60

Page intentionally blank

ABSTRACT

We conducted three annual airborne lidar surveys along the Texas Gulf shoreline in 2010, 2011, and 2012 to determine short-term shoreline change and its long-term context, map critical beach and dune attributes including the shoreline, potential vegetation line, and landward dune boundary, examine and quantify beach and dune morphology by determining elevation-threshold area (ETA) curves for differing geomorphic environments on the Texas coast, and establish a storm susceptibility index (SSI) for the Gulf shoreline.

On average, long-term shoreline change trends are erosional for all major Texas coastal segments. Over the short term, the Texas Gulf shoreline advanced an average of 6.5 m between 2010 and 2011, a period that was characterized by continued long-term recovery from Hurricane Ike (2008). The shoreline advanced at 75 percent of monitoring sites during this period. This trend largely reversed between 2011 and 2012, when the shoreline retreated at 67 percent of monitoring sites over an average distance of 3.1 m landward. Coastwide shoreline change patterns were similar to long-term trends during this period. The most stable or advancing shorelines were located on the central Texas coast. Shorelines along the upper and lower parts of the coast generally retreated. Predominant shoreline retreat between 2011 and 2012 did not fully offset advance in 2010 to 2011. Between 2010 and 2012, the shoreline advanced at 59 percent of sites over an average distance of 3.4 m, resulting in a net beach gain of 203 ha.

Digital elevation models (DEMs) constructed from airborne lidar data were used to determine elevation-threshold area (ETA) curves for major geomorphic units and each coastal county. Areas exceeding threshold elevations of 2 to 9 m (in 1-m increments) have characteristic shapes that are useful in determining sand storage volumes, susceptibility to storm flooding, and erosion resistance and recoverability. DEMs were also used to create an eight-level storm susceptibility index (SSI) that indicates the predicted protection level from storms at recurrence intervals of 1 to 200 years.

Page intentionally blank

INTRODUCTION

The Texas coastal zone (fig. 1) is among the most dynamic geologic environments on Earth. Shoreline and vegetation-line position and beach and dune morphology (height, width, and change over time) are critical parameters that reflect the balance among several important processes, including sea-level rise, land subsidence, sediment influx, littoral drift, and storm frequency, intensity, and recovery. Because the Texas coast faces ever-increasing developmental pressures as the coastal population swells, an accurate and frequent analysis of short- and long-term Gulf coast change can serve as a planning tool to identify areas of habitat gain or loss, better quantify erosion and storm flooding threats to residential, industrial, and recreational facilities and transportation infrastructure, and help understand the natural and anthropogenic causes of beach, dune, and vegetation change.

The latest trends in coastal change are critical components in understanding the potential impact that sea level, subsidence, sediment supply, and coastal engineering projects might have on growing coastal population and sensitive coastal environments such as beaches, dunes, and wetlands. Rapidly eroding shorelines threaten coastal habitat and recreational, residential, transportation, and industrial infrastructure and can also increase the vulnerability of coastal communities to tropical storms. Periodic analyses of shoreline, vegetation line, and dune position, rates of change, and factors contributing to coastal change give citizens, organizations, planners, and regulators an indication of expected future change and help determine whether those changes are accelerating, decelerating, or continuing at the same rate as past changes.

Historical change rates of the Texas Gulf shoreline were first determined by the Bureau of Economic Geology (Bureau) in the 1970s and presented in a series of publications covering the 332 mi (535 km) of Gulf shoreline (Morton, 1974, 1975, 1977; Morton and Pieper, 1975a, 1975b, 1976, 1977a, 1977b; Morton and others, 1976). This publication series presented net long-term change rates determined from shoreline positions documented on 1850 to 1882 topographic charts published by the U. S. Coast and Geodetic Survey (Shalowitz, 1964) and aerial

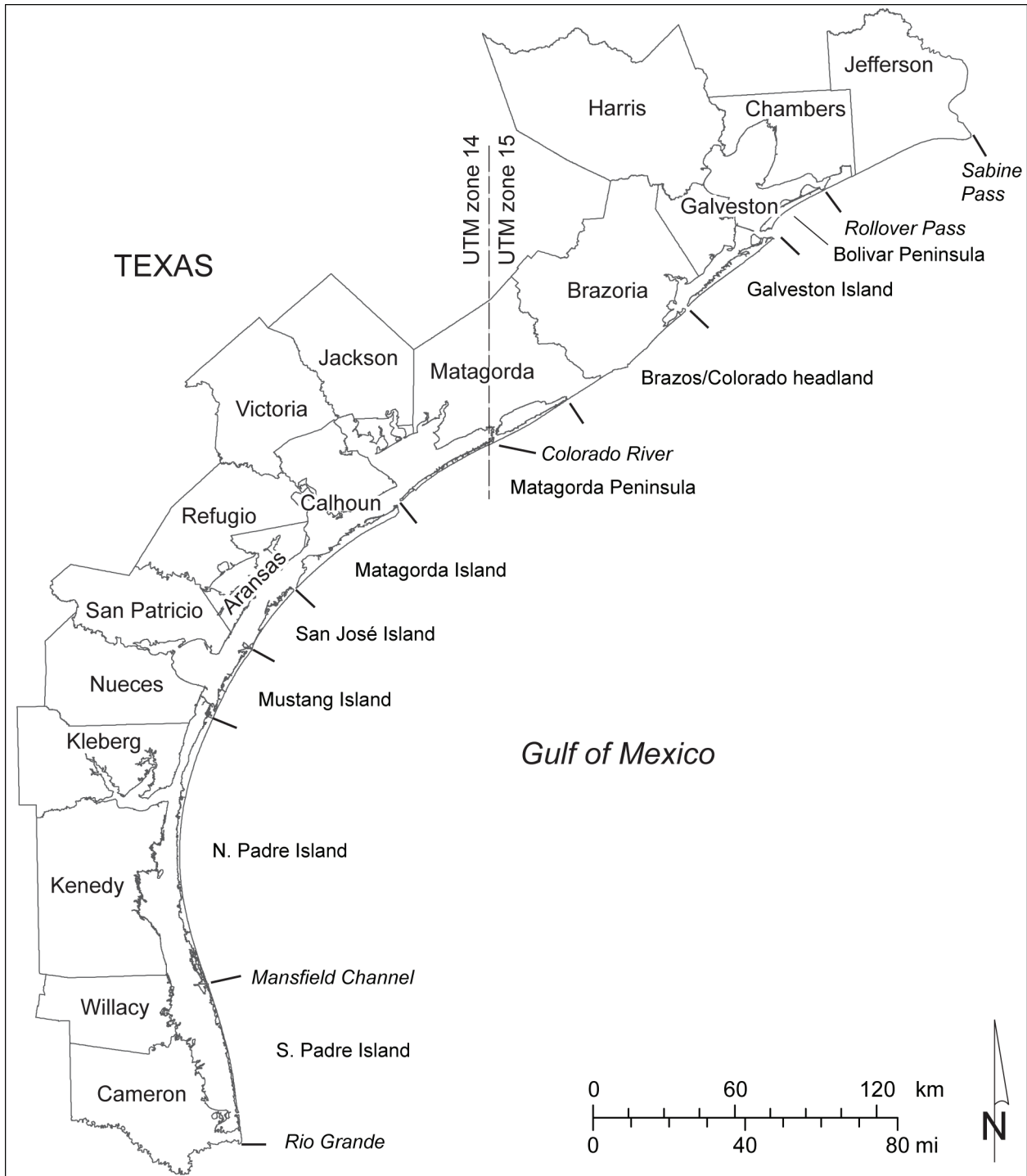


Figure 1. Map of the Texas coastal zone showing principal geomorphic features and coastal counties. Line segments extending seaward from the shoreline mark boundaries between major geomorphic features (barrier islands, peninsulas, deltaic headlands, and strandplains).

photographs acquired between about 1930 and 1975. Rates of change for the entire Gulf shoreline were updated through 1982 based on aerial photographs (Paine and Morton, 1989; Morton and Paine, 1990). Updates for subsets of the Texas Gulf shoreline include the upper coast between Sabine Pass and the Brazos River through 1996 (Morton, 1997) and the Brazos River to Pass Cavallo (Gibeaut and others, 2000) and Mustang and north Padre Island (Gibeaut and others, 2001) segments through 2000 using shoreline positions established using an airborne lidar topographic mapping system. Lidar-derived shoreline positions in 2000–2001 were also used as part of a Gulf-wide assessment of shoreline change that included the Texas coast (Morton and others, 2004). Coast-wide rates of historical shoreline change was recently updated using 2007 aerial photographs, the most recent coast-wide coverage predating Hurricane Ike in 2008 (Paine and others, 2011, 2012).

This report presents and discusses short-term shoreline, beach, vegetation, and dune changes and Gulf shore storm susceptibility determined from three annual airborne lidar surveys conducted by the Bureau in April 2010, April 2011, and February 2012. These surveys, conducted with field logistical assistance from Flight Services at the Texas Department of Transportation, the Center for Space Research at The University of Texas at Austin, Harte Research Institute (HRI) and Conrad Blucher Institute at Texas A&M University – Corpus Christi, and the National Geodetic Survey, flew a swath about 500-m wide along the entire Texas Gulf of Mexico shoreline that included the beach and major dunes landward of the beach. At the Bureau, lidar and associated GPS data were processed to produce full-resolution point cloud images and 1-m resolution digital elevation models (DEMs) of the ground surface. Bureau researchers determined shoreline position for each annual survey by extracting the 0.6-m msl elevation contour as the shoreline proxy. Bureau researchers determined shoreline change between each annual survey and for the entire monitoring period (2010 to 2012) and compared those changes to historical shoreline change rates. DEMs were also used by Bureau researchers to examine relationships in the coastal counties and along the principal geomorphic units in surface area above threshold elevations at

1-m intervals. Major differences in areas above threshold elevations for different parts of the coast indicate significant differences in sand storage, erosion resilience, and storm flooding susceptibility. Imagery and DEMs were used by Bureau and HRI researchers to determine landward dune boundaries and the potential vegetation line (PVL) boundary. Researchers at HRI determined storm susceptibility indices for the Gulf shoreline by determining morphologic similarities along the coast using the 1-m DEM.

There are many geologic, oceanographic, and meteorological factors that influence the position and health of the beach and dune system. Any analysis of position and movement of dynamic coastal features, particularly over a short period (two years in this study) must consider the conditions during the time the change was measured. Two of the more significant influences are relative sea-level change and storm incidence and intensity.

Relative Sea Level

Changes in sea level relative to the ground surface have long been recognized as a major contributor to coastal change (e.g. Bruun, 1954, 1962, 1988; Cooper and Pilkey, 2004). Rising sea level inundates low-relief coastal lands causing shoreline retreat by submergence, and elevates dynamic coastal processes (currents and waves) that can accelerate shoreline retreat by physical erosion. Changes in relative sea level include both changes in the ocean surface elevation (eustatic sea level) and changes in the elevation of the ground caused by subsidence or uplift. Eustatic sea-level change rates, established by monitoring sea level at long-record tide gauge stations around the world and more recently using satellite altimetry, vary over a range of about 1 to 4 mm/yr. Gutenberg (1941) calculated a eustatic rate of 1.1 mm/yr from tide gauge data. Estimates based on tide gauge data since then have ranged from 1.0 to 1.7 mm/yr (Gornitz and others, 1982; Barnett, 1983; Gornitz and Lebedeff, 1987; Church and White, 2006), although Emery (1980) supported a higher global average of 3.0 mm/yr that is comparable to more recent globally averaged, satellite-based rates. Attempts to remove postglacial isostatic movement and geographical bias

from historical tide gauge records resulted in eustatic estimates as high as 2.4 mm/yr (Peltier and Tushingham, 1989). Recent studies that include satellite altimetry data acquired since 1993 indicate that global rates of sea-level rise average 2.8 mm/yr, or 3.1 mm/yr with postglacial rebound removed (Cazenave and Nerem, 2004). Much of this recent rise is interpreted to be caused by thermal expansion of the oceans with a possible contribution from melting of glaciers and polar ice (FitzGerald and others, 2008; Cazenave and Nerem, 2004; Leuliette and Miller, 2009).

In major sedimentary basins such as the northwestern Gulf of Mexico, eustatic sea level rise is augmented by subsidence. Published rates of relative sea-level rise measured at tide gauges along the Texas coast are higher than eustatic sea-level rates (Swanson and Thurlow, 1973; Lyles and others, 1988; Penland and Ramsey, 1990; Paine, 1991, 1993), ranging from 3.4 to 6.5 mm/yr between 1948 and 1986 for tide gauges at Galveston Pier 21, Rockport, and Port Isabel. These gauges represent single points along the coast and may not be representative of relative sea-level rise along the entire coast. Geodetic releveling data obtained from the National Geodetic Survey at benchmarks along the Texas coast from Galveston Bay to Harlingen show local variation in subsidence rates that would produce average rates of relative sea-level rise ranging from about 2 to more than 20 mm/yr. Despite the wide range, most of the rates fall within the range observed for the long-term Texas tide gauges, suggesting that the gauges are representative regional indicators of relative sea-level rise (Paine, 1991, 1993).

The most recent relative sea-level rise rates from selected Texas tide gauges range from 1.93 to 6.61 mm/yr (fig. 2, table 1). These rates were calculated by the National Oceanic and Atmospheric Administration through 2012 from periods of record that begin between 1908 (Galveston Pier 21) and 1963 (Port Mansfield). The highest rates (above 5 mm/yr) are calculated for upper and central Texas coast tide gauges at Galveston (Pier 21 and Pleasure Pier), Sabine Pass, and Rockport. The lowest rate (1.93 mm/yr) is calculated for Port Mansfield, which also has the shortest record. The remaining gauges (Port Isabel, North Padre Island, and Freeport) have rates between 3.48 to 4.35 mm/yr.

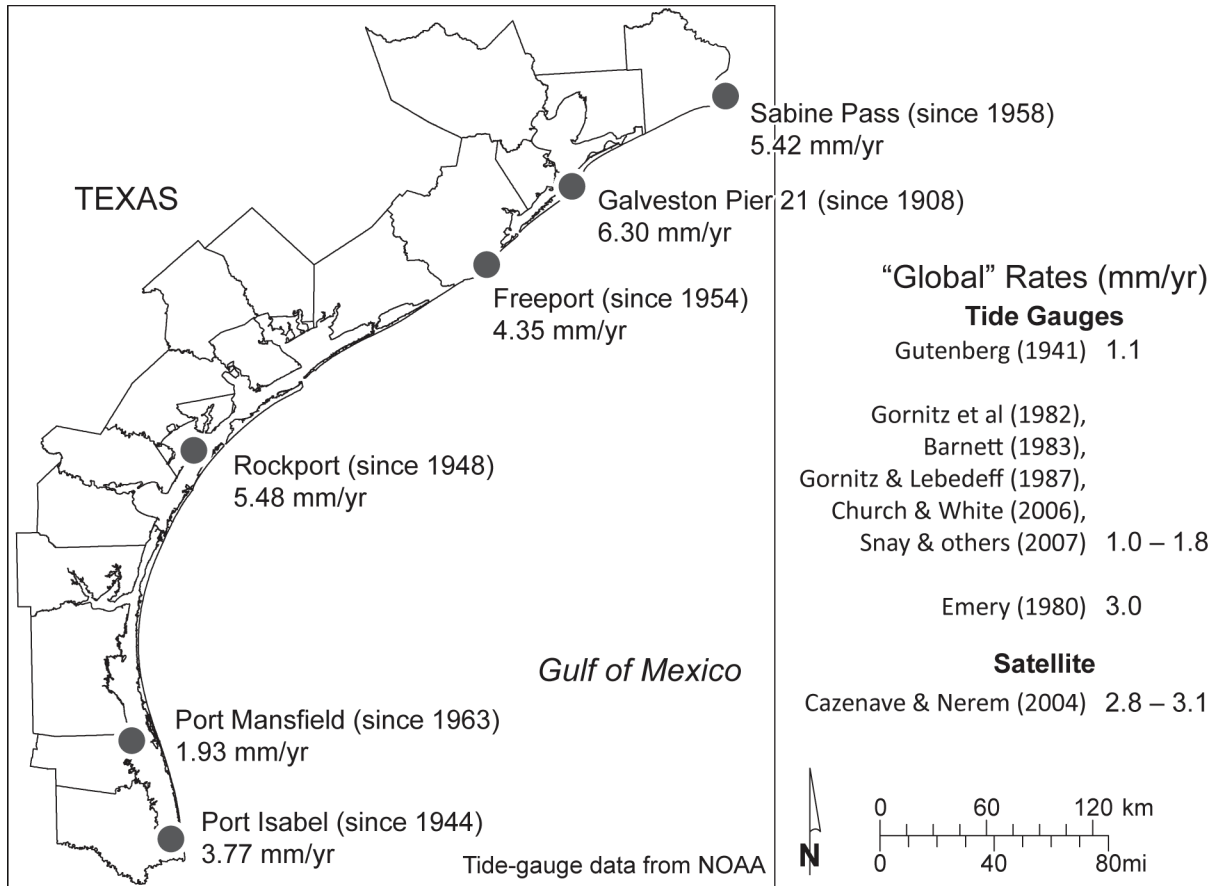


Figure 2. Sea-level trend at selected Texas tide gauges through 2012 and “global” rates determined from tide gauges and satellite data. Texas tide-gauge data from National Oceanic and Atmospheric Administration.

Table 1. Long-term rates of relative sea-level rise at select Texas tide gauges (fig. 2) through 2012. Data from National Oceanic and Atmospheric Administration.

Gauge	Beginning year	Period	Rate (mm/yr)	95% confidence interval (mm/yr)
Sabine Pass	1958	55	5.42	0.86
Galveston Pier 21	1908	105	6.35	0.26
Galveston Pleasure Pier	1957	55	6.61	0.70
Freeport	1954	53	4.35	1.12
Rockport	1948	65	5.48	0.57
Port Mansfield	1963	44	1.93	0.97
Padre Island	1958	49	3.48	0.75
Port Isabel	1944	69	3.77	0.37

Galveston Pier 21 has the longest period of record. Long-term rates of sea-level rise calculated from monthly averages of sea level between April 1908 and April 2011 (fig. 3) are 6.3 mm/yr, similar to the NOAA-calculated rate through 2012 (table 1). Sea-level rise at this gauge has not been constant. Calculations of average rate of change over a rolling 19-year window (chosen to match the duration of the 19-year National Tidal Datum Epoch and centered on the mid-date) show multiyear oscillations in average rate that range from 1.0 to 13.3 mm/yr (fig. 3). The most recent rates (since about 1990) are 2.2 to 4.1 mm/yr, among the lowest observed at the gauge, and are similar to satellite altimetry-based eustatic rates for the same period. The period of the airborne lidar surveys (April 2010 to February 2012) coincides with a period of relative sea-level stability as measured at Galveston Pier 21.

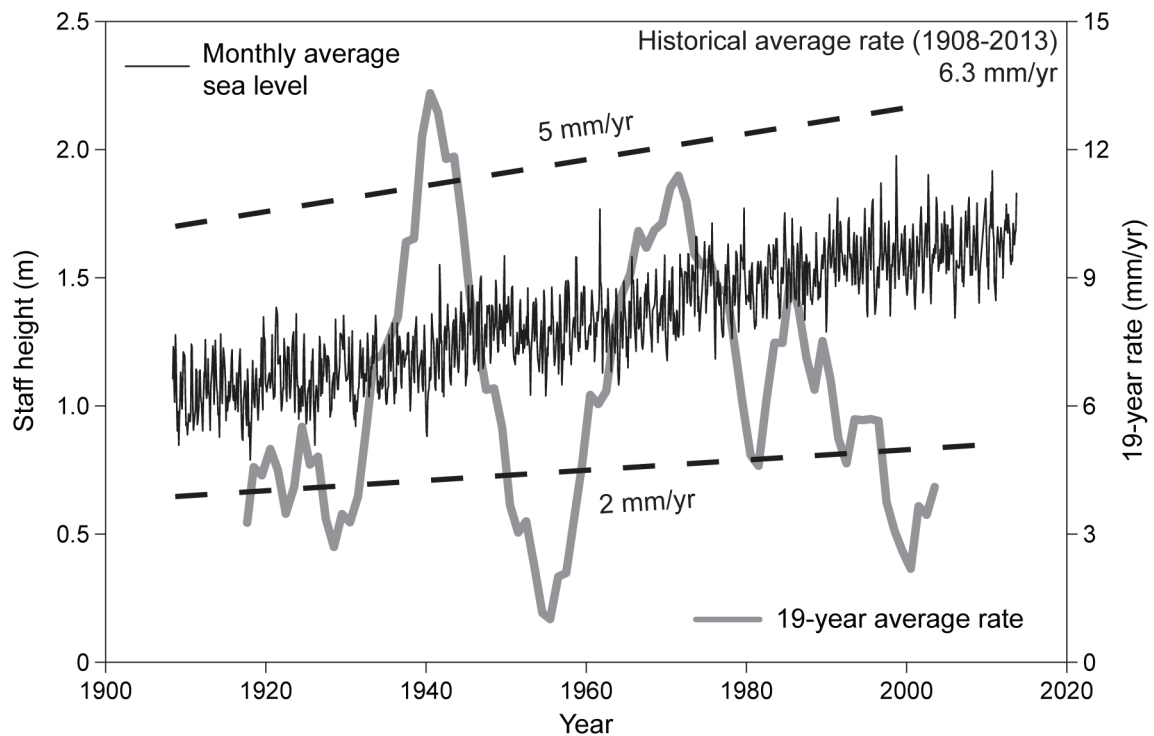


Figure 3. Sea-level trend at Galveston Pier 21, 1908 to 2013. Black line is monthly average sea level. Gray line is the average sea level measured over a 19-year period (the tidal datum epoch) and plotted at the center date of the period. Dashed lines indicate the slope of long-term rise at 2 mm/yr and 5 mm/yr. Data from National Oceanic and Atmospheric Administration.

Tropical Cyclones

There are numerous examples of the impact that tropical cyclones (tropical storms and hurricanes) have on the Texas Gulf shoreline (e.g. Price, 1956; Hayes, 1967; Morton and Paine, 1985). These include tropical storms and hurricanes that are classified following the Saffir/Simpson hurricane wind scale (Simpson and Riehl, 1981). In general, minimum central pressures decrease as the categories increase, as does pressure- and wind-driven storm surge. Two critical parameters that influence the erosion potential of a tropical cyclone are surge height and surge duration: the longer sea level is elevated above normal during storm passage, the greater the potential for redistribution of sediment eroded from the beach. Beach and dune recovery after storm passage follows several distinct stages and can take years (Morton and Paine, 1985; Morton and others, 1994). The initial airborne lidar survey for this project was April 2010, which allowed about 1.5 years of coastal recovery following Hurricane Ike (2008).

Historical lists (Roth 2010) and records maintained by the National Oceanic and Atmospheric Administration enumerate 64 hurricanes and 57 tropical storms that have struck the Texas coast from 1850 through 2013. On average, four hurricanes and four tropical storms make landfall in Texas per decade. The longest hurricane-free period in Texas lasted nearly 10 years from October 1989 to August 1999 (Roth, 2010). From 2007 through 2013, the period most applicable to this study, 7 tropical cyclones have crossed the Texas coast (table 2). This includes 4 tropical storms and 3 hurricanes that were Category 1 (Humberto, 2007) or Category 2 (Dolly and Ike, 2008) at landfall. Notable among these is Hurricane Ike, once a Category 4 storm that severely eroded middle and upper Texas coast beaches as a very large Category 2 storm associated with an unusually high and long-duration storm surge in September 2008. During the airborne lidar survey period, only Tropical Storm Hermine (September 2010) and Tropical Storm Don (July 2011) crossed the Texas coast. Hermine made landfall on the northeastern coast of Mexico near Matamoros on September 7, 2010, accompanied by winds of 110 km/hr and surge heights of 0.5 to 1.0 m along the south Texas coast near the landfall area (Avila, 2010). Don weakened to a tropical depression as it made landfall along Padre Island National Seashore just northeast of

Table 2. Tropical cyclones affecting the Texas coast between 1990 and 2013. TS = tropical storm; H = hurricane; number following H designates numeric strength according to the Saffir/Simpson scale (Simpson and Riehl, 1981). Data from the National Oceanic and Atmospheric Administration and Roth (2010). Tropical storms Hermine (2010) and Don (2011) were the only cyclones to make landfall in Texas during the 2010 to 2012 project period.

Year	Category	Name	Begin date	End date	Landfall area
1993	TS	Arlene	6/18/1993	6/21/1993	North Padre Island
1995	TS	Dean	7/28/1995	8/2/1995	Freeport
1998	TS	Charley	8/21/1998	8/24/1998	Aransas Pass
1998	TS	Frances	9/8/1998	9/13/1998	Matagorda Island
1999	H4	Bret	8/18/1999	8/25/1999	Padre Island (weakened)
2001	TS	Allison	6/5/2001	6/17/2001	Freeport
2002	TS	Bertha	8/4/2002	8/9/2002	North Padre Island
2002	TS	Fay	9/5/2002	9/8/2002	Matagorda Peninsula
2003	H1	Claudette	7/8/2003	7/17/2003	Matagorda Peninsula
2003	TS	Grace	8/30/2003	9/2/2003	Galveston Island
2005	H5	Rita	9/18/2005	9/26/2005	Sabine Pass (H3 at landfall)
2007	TS	Erin	8/15/2007	8/17/2007	San Jose Island
2007	H1	Humberto	9/12/2007	9/14/2007	Upper Texas coast
2008	H2	Dolly	7/20/2008	7/25/2008	South Padre Island
2008	TS	Edouard	8/3/2008	8/6/2008	Upper Texas coast
2008	H4	Ike	9/1/2008	9/15/2008	Galveston (H2 at landfall)
2010	TS	Hermine	9/5/2010	9/9/2010	Rio Grande area
2011	TS	Don	7/27/2011	7/29/2011	Baffin Bay area (TD at landfall)

Baffin Bay on July 30, 2011 (Brennan, 2011). The maximum recorded surge height was 0.6 m at Bob Hall Pier (Brennan, 2011).

METHODS

Principal project tasks included (1) planning three annual airborne topographic lidar surveys of a swath along the entire Texas Gulf shoreline, (2) acquiring and processing the airborne lidar data, (3) producing full-resolution point clouds and digital elevation models (DEMs) for the three surveys, (4) extracting a shoreline proxy at 0.6 m elevation from the DEMs to analyze short- and long-term shoreline change, (5) mapping the potential vegetation line, the landward dune boundary, and determining a storm susceptibility index for the Texas Gulf shoreline, and (6) analyzing DEMs to assess sand storage, storm surge flood susceptibility, and coastal erosion resilience.

Lidar Data Acquisition

Researchers from the Bureau, the Center for Space Research, and Texas A&M–Corpus Christi completed three airborne lidar surveys of the Texas Gulf of Mexico shoreline from Sabine Pass to the Rio Grande. The lidar system (Optech Inc. ALTM 1225, serial number 99d118) was installed in a single engine Cessna Stationaire 206 aircraft (tail number N147TX) owned and operated by the Texas Department of Transportation, and operated out of Galveston, Rockport, and Harlingen, Texas. Lidar instrument settings for these flights were: laser pulse rate: 25 kHz; scanner rate: 26 Hz; scan angle: +/-20 degrees; beam divergence: narrow; altitude: 570 to 1200 m AGL (dependent upon cloud level); and ground speed: 70 to 120 kts.

The 2010 survey required five days of flying between April 8 and 24 (fig. 4). Data collection on other days within that period was hindered by poor weather. Data were collected on the upper Texas coast from Sabine Pass to San Luis Pass on April 8, from Bolivar Roads to the mouth of the Colorado River on April 9 (two passes on Galveston Island on both April 8 and 9), and from the mouth of the Colorado River to Aransas Pass on April 10. Following a break for poor weather, surveying resumed on April 21 from Aransas Pass to Mansfield Channel. The final segment, from Mansfield Channel to the Rio Grande, was flown on April 24.

April 8, 2010 = Julian day 09810

April 9, 2010 = Julian day 09910

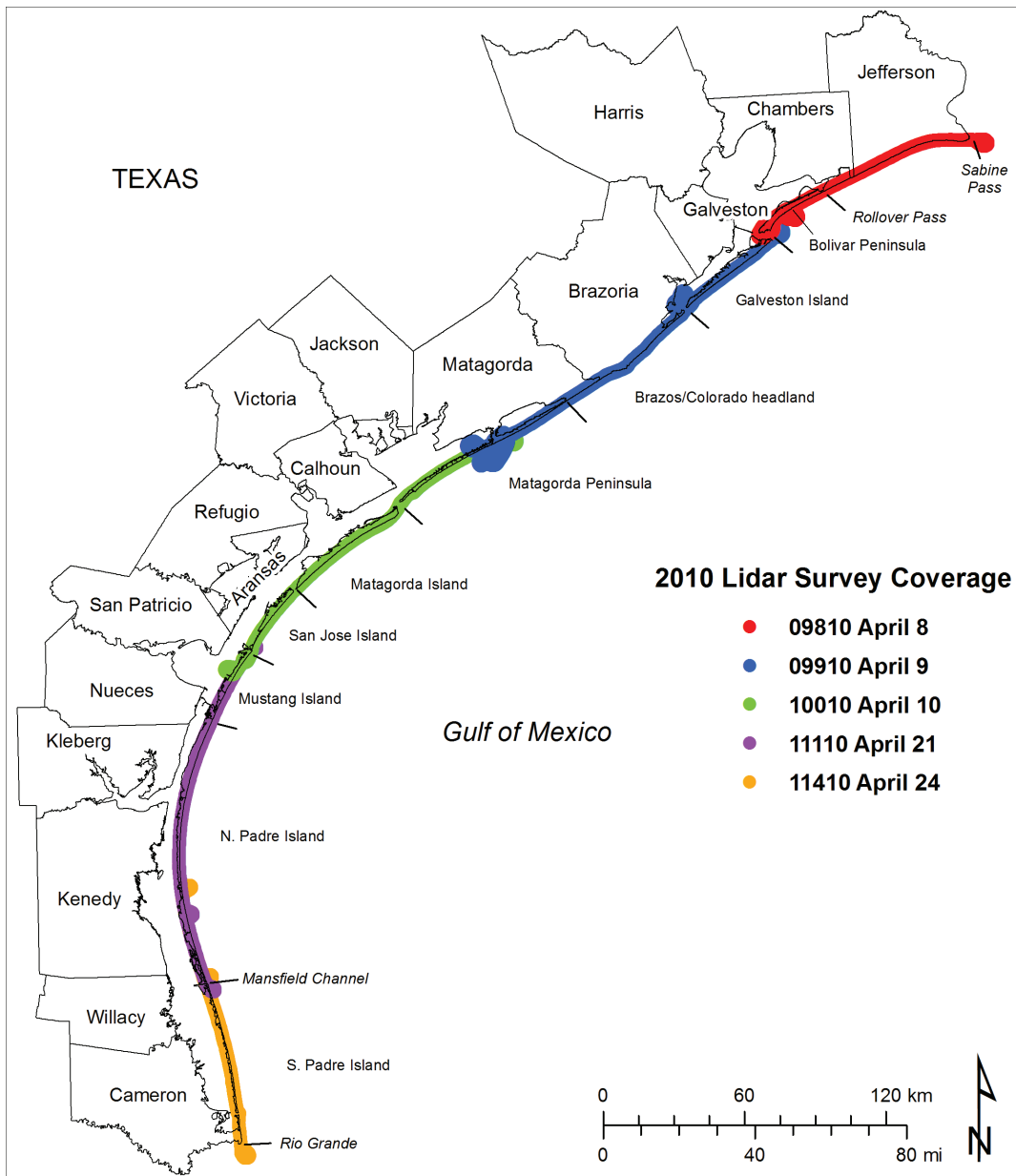


Figure 4. Coverage map of the 2010 lidar survey.

April 10, 2010 = Julian day 10010
April 21, 2010 = Julian day 11110
April 24, 2010 = Julian day 11410

The 2011 survey required six days of flying between April 6 and 16 (fig. 5). Data collection on other days within that period was hindered by poor weather. Data were collected in the coastal bend from Aransas Pass to Baffin Bay on April 6 and from Baffin Bay to Mansfield Pass (Padre Island) on April 7 (two passes). Following a break for poor weather, surveying resumed on April 12 from Sabine Pass to the Brazos River, on April 13 from the Brazos River to Pass Cavallo, and on April 15 from Pass Cavallo to Aransas Pass. The final segment, from Mansfield Channel to the Rio Grande, was flown on April 16.

April 6, 2010 = Julian day 09611
April 7, 2010 = Julian day 09711
April 12, 2010 = Julian day 10211
April 13, 2010 = Julian day 10311
April 15, 2010 = Julian day 10511
April 16, 2010 = Julian day 10611

The 2012 survey required six days of flying between February 14 and 26 (fig. 6). Data collection on other days within that period was hindered by poor weather. Data were collected on Galveston Island on February 14, Bolivar Peninsula on February 16, and Matagorda Peninsula on February 19. Follets Island, Matagorda Peninsula, and Matagorda Island were flown during two flights on February 20. Following a break for poor weather, surveying resumed February 26 with two data collection sessions covering San José, Mustang, and North Padre Islands. The final segment of Padre Island (Baffin Bay area) to the Rio Grande was surveyed during two flights on February 27.

February 14, 2012 = Julian Day 04512
February 16, 2012 = Julian Day 04712
February 18, 2012 = Julian Day 04912
February 19, 2012 = Julian Day 05012
February 25, 2012 = Julian Day 05612
February 27, 2012 = Julian Day 05712

Twelve GPS base station locations were used during the surveys. The base stations were at the following locations: High Island (HIGH), Fort Travis County Park (CG11), Scholes Field

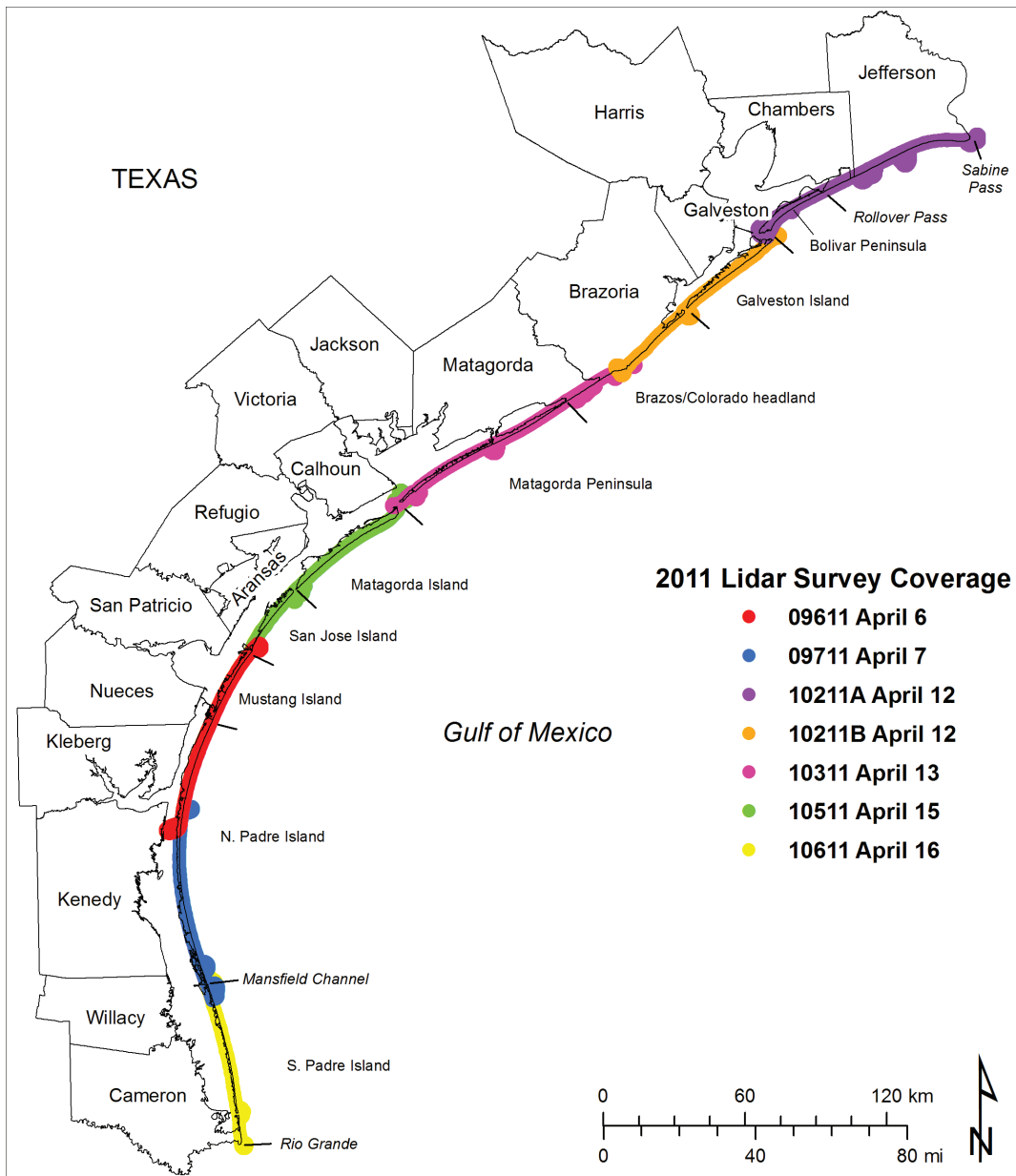


Figure 5. Coverage map of the 2011 lidar survey.

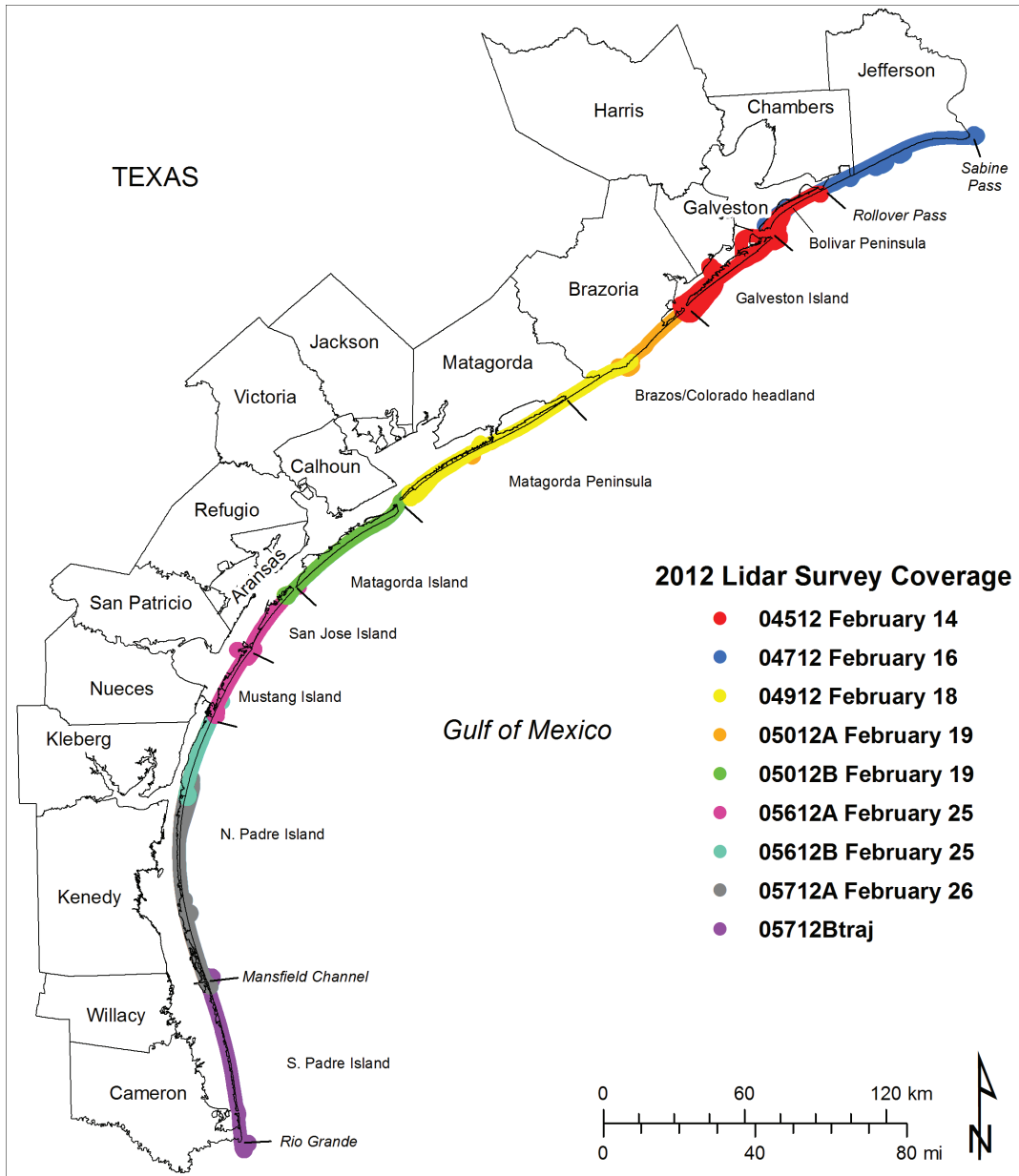


Figure 6. Coverage map of the 2012 lidar survey.

Galveston Airport (GLS1), Surfside (SURF), Matagorda Bay Nature Park (IDOL), Seadrift (SEAD), Port Aransas (PTAR), Bob Hall Pier (HOLI), Padre Island National Seashore (PINS), Port Mansfield (PTMN), South Padre Island Convention Center (SPI1), and U.S. Coast Guard Station at South Padre Island. All base station data (table 3) are reported in NAD83. Ellipsoid heights are relative to the GRS80 ellipsoid.

Additionally, Continuously Operating Reference Stations (CORS) at Port Arthur, Galveston, and Port Aransas were set by the Texas Department of Transportation and the National Geodetic Survey to record data at 1-second interval.

Lidar Data Processing

While in the field, raw ALTM 1225 flight data (laser ranges with associated scan angle information and IMU data), airborne GPS data collected at 1 Hz using an Ashtech receiver, and ground-based GPS data collected at 1 Hz using Ashtech Z-12 receivers are transferred to a computer. A decimated lidar point file is generated from the above three data sets using Optech's Realm 2.27 software. This is a 9-column ASCII data set with the following format: time tag; first return Easting, Northing, HAE; last return Easting, Northing, HAE; first return intensity; and last return intensity. The decimated lidar point file is reviewed to check data coverage (such as sufficient overlap of flight lines and point spacing).

Base station coordinates are computed using National Geodetic Survey's Online Positioning User Service (OPUS) software. Aircraft trajectories for each base station are computed using National Geodetic Survey's KINPOS software. Solutions for each base station coordinates and aircraft trajectories are in the International Terrestrial Reference Frame of 2000 (ITRF2000). Trajectories from each base station are merged into one for each flight. Weighting for the trajectory merge is based upon baseline length (distance from base station) and solution RMS errors. The trajectory solution is transformed from ITRF 2000 to North American Datum of 1983 (NAD83) using the National Geodetic Survey's Horizontal Time Dependent Positioning software. The NAD83

Table 3. GPS base stations used during the 2010, 2011, and 2012 airborne lidar surveys.

Station ID	Latitude (N)	Longitude (W)	HAE (m)	Julian day (2010)	Julian day (2011)	Julian day (2012)
HIGH	29 33 25.92707	94 23 43.98956	-21.970	098	102	045, 047
CG11	29 21 47.90532	94 45 30.41189	-22.393	098		045
GLS1	29 16 11.08755	94 51 28.66116	-25.376	098, 099	102, 103	045, 047, 049
SURF	28 57 9.17032	95 17 10.82111	-24.742	099	102, 103	047, 049, 050
IDOL	28 35 53.98620	95 58 38.56969	-24.368	099, 100	103	049, 050
SEAD	28 24 29.83512	96 42 47.40918	-24.992	100	103, 105	050
PTAR	27 50 22.06971	97 04 20.59319	-24.521	100, 111	096, 105	056
HOLI	27 35 12.20372	97 13 16.44379	-23.994	111		056, 057
PINS	27 25 18.19210	97 18 36.37265	-21.646		096, 097, 116	
PTMN	26 33 25.87875	97 25 44.76583	-19.507	111, 114	097, 106	057
SPI1	26 8 29.57345	97 10 22.28338	-20.606		097	057
USCG	26 04 26.04962	97 09 53.75090	-20.667	114	106	

trajectories and aircraft inertial measurement unit data are input into Applanix's POSProc version 2.1.4 to compute an optimal 50 Hz inertial navigation solution (INS) and smoothed best estimate of trajectory (SBET). The new INS and SBET are substituted into Realm 2.27 to generate a set of initial lidar instrument calibration parameters (pitch, roll, and scale) for each lidar flight. The parameters are incrementally improved by iteratively comparing a subset of the lidar output to GPS kinematic ground control.

Ground GPS surveys were conducted within the lidar survey area to acquire ground-truth information. The ground survey points are estimated to have a vertical accuracy of 0.01 to 0.05 m. Roads and open areas with an unambiguous surface were surveyed using kinematic GPS techniques. A lidar data set was then sorted to find data points that fall within 0.5 m of a ground GPS survey point. The mean elevation difference between the lidar and the ground GPS was used to estimate and remove an elevation bias from the lidar data. The standard deviation of these elevation differences provides estimates of the lidar precision. Vertical biases were determined for and removed from each flight (numbered by Julian day) (table 4). Once the instrument calibration parameters are sufficiently accurate, a complete lidar point file (9-column ASCII file) was created for the entire survey area and the point files were transferred to a UNIX workstation.

The 9-column lidar point files were parsed into 3.75-minute quarter-quadrangle components and bias corrections were applied to the first and last returns. Two deliverable formats were created from the bias corrected point files: (1) LAS point files, and (2) DEMs. The ASCII point files are geoid corrected and converted to LAS 1.2 format using ASPRS specifications. The quarter-quadrangles are merged into quadrangle files for LAS format data delivery.

The bias corrected quarter-quadrangle point files were also gridded to create DEMs with software written at the Bureau. This in-house gridding software uses a weighted inverse distance algorithm to interpolate cell values. The Geoid99 geoid model was applied to the grids to convert z-values from height above the GRS80 Ellipsoid to elevations with respect to the North Ameri-

Table 4. Bias corrections and standard deviations for the 2010, 2011, and 2012 airborne lidar surveys.

Year	Julian day	First return	RMS error	Last return	RMS error
2010	09810	-0.0772	0.0387	-0.0973	0.0580
	09910	-0.1169	0.0550	-0.1106	0.0750
	10010	-0.1363	0.0840	-0.1157	0.0990
	11110	-0.1803	0.0450	-0.1538	0.0530
	11410	0.0589	0.0510	0.0708	0.0690
2011	09611	-0.0886	0.0446	-0.0905	0.0638
	09711	0.2036	0.1236	0.2190	0.1313
	10211A	-0.1595	0.0436	-0.1685	0.0618
	10211B	-0.1275	0.0607	-0.1280	0.0726
	10311A	-0.1566	0.0319	-0.1488	0.0491
	10311B	-0.1569	0.0296	-0.1538	0.0569
	10511	-0.2109	0.0520	-0.1916	0.0666
	10611	0.1240	0.0482	0.1291	0.0616
2012	04512	-0.0830	0.0571	-0.0763	0.0720
	04712	-0.1029	0.0522	-0.0978	0.0699
	04912	-0.1046	0.0399	-0.1057	0.0587
	05012A	-0.1281	0.0381	-0.1467	0.0593
	05012B	0.1234	0.0382	0.1316	0.0625
	06512A	-0.1236	0.0431	-0.1460	0.0630
	05612B	-0.1210	0.0423	-0.1424	0.0614
	05712A	-0.1097	0.0372	-0.1226	0.0533
	05712B	0.2292	0.0584	0.2288	0.0773

can Vertical Datum 88 (NAVD88). The program simultaneously grids four data attributes: first return z, first return intensity, second return z, and second return intensity.

The grid files were then output into one of two formats: (1) an ASCII raster file or (2) a raw 4-byte binary raster file. Using the ASCII format, each one of the four attributes listed above must be output to a separate file for import into ArcGIS. This format consists of a matrix of attribute values preceded by six lines of header information including: number of columns, number of rows, x coordinate of the lower-left cell, y coordinate of the lower-left cell, cell size, and null value. Using the binary format, generates multi-band, band interleave files containing one, two, three, or all four of the attribute data referenced above. Additionally, a header file in ERMapper's ".ers" format for each of the binary files is generated that allows the data to be viewed in ERMapper or ArcGIS. These header files contain the same information as the ASCII-format header files (except the coordinate values are of the upper-left cell) plus datum and projection information.

Shoreline

Before the advent of airborne lidar, vertical aerial photography was commonly used to map shoreline position. Shorelines were drawn or digitized on the photography, generally at the distinct tonal boundary between wet and dry sand on the beach. The position of this boundary can vary due to water level, wave activity, and georeferencing errors. Through analysis of lidar surveys and beach profiles, Gibeaut and others (2002) and Gibeaut and Caudle (2009) determined that the wet/dry boundary occurs at about 0.6 m above local mean sea level (msl). Using the most seaward, continuous contour of 0.6 m msl provides a consistent shoreline feature between lidar data sets when water level and wave activity may differ.

At the Bureau, the 2010, 2011, and 2012 DEMs were opened in ESRI ArcMap software and 0.6 m was calculated and displayed. The file was edited to retain the most seaward, continuous contour. The extracted contour was smoothed in ArcMap using the "Smooth Line" function

(PAEK algorithm with a 2-m smoothing tolerance). The number of vertices in the polyline were reduced by using ET Geowizards “Generalize Polyline” command with a 0.25 m tolerance. This retains the shape of the smoothed polyline while reducing the number of vertices. Topology errors were removed including dangles, self-overlapping lines, and self-intersecting lines. Adjacent line segments were aggregated using ArcMap “Unsplit Line” function. Shoreline change between each pair of shorelines was calculated using the Digital Shoreline Analysis System as an ArcGIS extension (Thieler and others, 2009).

Potential Vegetation Line

Mapping the natural line of vegetation from aerial photographs has proven difficult when establishing a legal boundary for the Texas Open Beaches Act (OBA). Gibeaut and Caudle (2009) sought to establish a consistent mapping technique based on lidar elevation data that can be used to determine the “potential vegetation line” or PVL. A statistical analysis of long-term beach profile elevation data suggested that 1.2 m msl is the lowest elevation that foredune vegetation may form a continuous cover. The analysis only considered beach profiles from the Texas coast with natural dunes. The most seaward 1.2 m contour line extracted from DEMs will either be within the vegetation or coincide with the vegetation line. Where it falls seaward of the vegetation, it indicates the potential position where natural vegetation and foredunes may advance.

The seaward boundary of the potential vegetation line was mapped at the Bureau as a contour line at 1.2 m msl on the 2010, 2011, and 2012 lidar DEMs. The 1.2 m elevation contour was calculated from the DEM using the contour function in ArcGIS. The relatively continuous contour line along the back edge of the beach and seaward edge of the foredune was selected as the potential vegetation line. The extracted contour was then smoothed in ArcMap using the “Smooth Line” function (PAEK algorithm with a 2 m smoothing tolerance). The number of vertices in the polyline are reduced by using ET Geowizards “Generalize Polyline” command with a 0.25 m tolerance. This retains the shape of the smoothed polyline while reducing the number of vertices.

Topology errors were removed including dangles, self-overlapping lines, and self-intersecting lines. Adjacent line segments were aggregated using ArcMap “Unsplit Line” function.

Landward Dune Boundary

The position of the landward dune boundary is an important factor in determining the space required for foredune formation, defining the foredune for volumetric and geomorphic analysis of the foredune, and also for use in determining design setback distances or creating foredune restoration projects. An automated process for selecting the boundary is not effective because the landward dune boundary is based upon qualitative criteria that are interpreted by examining a combination of lidar data and aerial photography. The following criteria were used for mapping the 2010, 2011, and 2012 landward dune boundary: (1) a change in slope from steep on the foredune to gentle on the back barrier; (2) elevation generally 2 m msl; (3) provides storm-surge protection; (4) morphology is elongate parallel to the shoreline; (5) proximity to the shoreline and other forms classified as foredunes; (6) connection to other forms classified as foredunes; and (7) density of clusters of dune forms (Gibeaut and Caudle, 2009).

The landward dune boundary was manually digitized at a scale of 1:800 to 1:1000. The foredune complex was defined as the most seaward, continuous feature with an elevation of at least 2 m. If a single continuous feature is not present, dune clusters are considered as part of the complex as long as they are quasi-perpendicular to the shore, close together, or connected. In areas where dunes are not present (such as washover areas), the dune boundary is mapped as the landward contour equivalent to the height of the vegetation line (1.2 m msl). Raster files representing hillshade, slope, and aspect of the DEM were used to help determine the extent of the dune boundary by visualizing the landward slope of dune features. In addition, aerial imagery was used to locate the extent of vegetation and to help identify man-made structures. Man-made structures are not considered to be part of the foredune complex; the dune boundary is placed seaward of any building or seawall. Adjacent line segments were aggregated using ArcMap “Unsplit Line” function.

Storm Susceptibility Index

Researchers at Harte Research Institute (HRI), Texas A&M–Corpus Christi developed the Storm Susceptibility Index for the project under a subcontract to the Bureau. The level of storm protection provided by beaches and dunes depends on their physical characteristics (dune height, width, and location) as well as the storm’s parameters such as surge elevation, wave height, and duration (Sallenger, 2000; Pries and others, 2008, Stockdon and others, 2009). The storm susceptibility index (SSI) estimates potential protection based on a model that incorporates beach and dune dimensions and location as predictors of expected protection given a set of storm surge and wave characteristics. The classification indicates the relative level of protection among profiles of the study area and does not consider wind damage, the type of built or natural environment being protected, potential return flow, or alongshore sediment transport effects during a storm.

Changes in the representative profiles resulting from a storm event were simulated using the SBEACH (Storm-induced BEACH CHange) model. The theoretical level of storm protection was determined by assessing beach and dune profile changes after simulating a set of synthetic storms and identifying the storm return period at which profiles are overwashed. Results of the assessment were extrapolated along the study area by matching representative pre-storm profiles to areas with similar beach and dune profile characteristics. Details of the SBEACH modeling effort at HRI are in Appendix B.

TEXAS GULF SHORELINE CHANGE

Short-term shoreline change determined at the Bureau from the three annual airborne lidar surveys in 2010, 2011, and 2012 are presented and analyzed in the context of long-term, historical shoreline change rates that were recently updated through 2007 (Paine and others, 2011, 2012). These long-term rates of Gulf shoreline change, calculated from multiple shoreline positions between the 1930s (mid- to late 1800s in some areas) and 2007, averaged 1.3 m/yr of retreat (fig. 7) for both net rate and linear regression rate calculations. Updated long-term rates were calculated at 11,731 sites along the entire Texas coast spaced at 50 m intervals. Net retreat occurred at 9,830 sites (84 percent) and advance occurred at 1,880 sites (16 percent). The overall rate is lower than the average change rate (retreat at 1.7 m/yr) determined from a previous update (through the mid 1990s to 2000), but the previous rates exclude central and lower coast segments on San José, Matagorda, and central Padre Islands that have generally low rates of change (slow advance to slow retreat). Shorelines along the upper Texas coast (from Sabine Pass to the mouth of the Colorado River) generally retreated at greater rates than those on the central and lower coast. Averages of change rates were retreat at 1.6 m/yr for the upper coast and retreat at 1.0 m/yr for the central and lower coast.

Notable extensive areas of relatively high long-term retreat rates include (1) the Sabine Pass to High Island area, (2) an area on Galveston Island west of the Galveston seawall, (3) the combined deltaic headland of the Brazos and Colorado rivers, (4) Matagorda Peninsula west of the Colorado River, (5) San José Island, and (6) the northern part and most of the southern half of Padre Island (fig. 7). Areas of general net shoreline advance are found (1) on the upper coast near the Sabine Pass and Bolivar Roads jetties, (2) at the western tip of Galveston Island, (3) on the Brazos/Colorado deltaic headland near the mouth of the Brazos River, (4) toward the western end of Matagorda Peninsula, (5) on the central Texas coast along much of Matagorda Island and near Aransas Pass, and (6) on Padre Island near Baffin Bay and the southern end of the island.

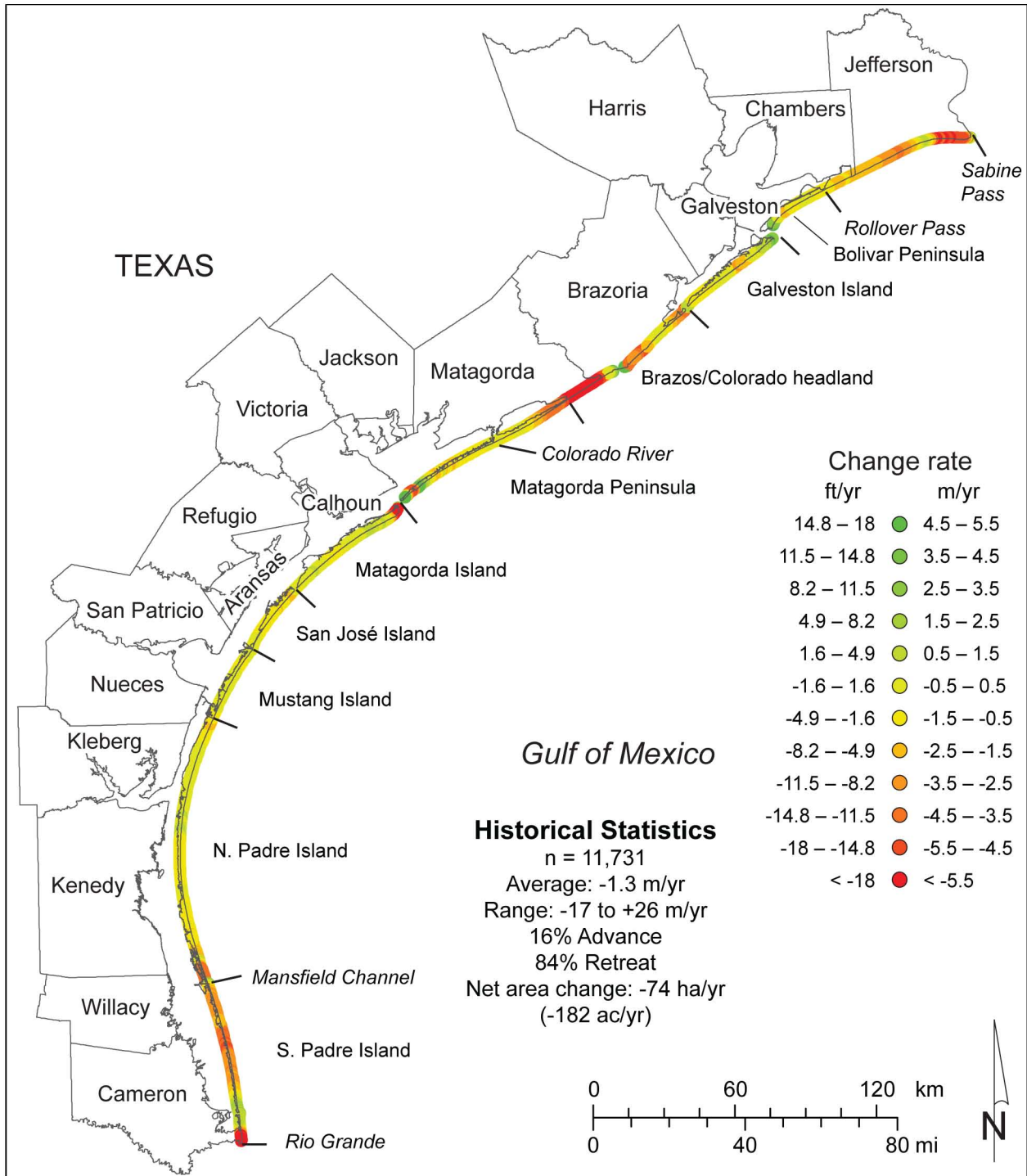


Figure 7. Net rates of long-term change for the Texas Gulf shoreline between Sabine Pass and the Rio Grande calculated from shoreline positions through 2007 (updated from Paine and others, 2011, 2012). Rates of change were calculated at 11,731 measurement sites spaced at 50-m intervals along the Gulf shoreline.

Closely spaced measurement sites allow estimates of long-term land loss to be made. The average annual rate of land loss along the Texas Gulf shoreline is 74 ha/yr. Total Texas Gulf shoreline land loss from 1930 through 2007 is estimated to be 5,670 ha.

Short-term Shoreline Change, 2010 to 2012

We determined short-term shoreline change for the three annual airborne lidar surveys by (1) extracting the 0.6-m msl elevation contour from each data set and using that as the shoreline proxy and (2) calculating distances between each shoreline (2010 to 2011, 2011 to 2012, and 2010 to 2012) at more than 11,000 measurement locations spaced at 50-m intervals along the Texas Gulf shoreline. Because rates of change have little meaning over such short time periods, change is presented as a distance rather than a rate.

Incremental Change between 2010 and 2011

The Texas Gulf shoreline predominantly advanced between airborne lidar surveys acquired in April 2010 and April 2011 (fig. 8). Change measured along the coast was positive (advancing) at 75 percent of the 11,783 of the measurement sites; the average distance that the shoreline advanced was 6.5 m. There was a net beach-area gain during this period of 382 ha.

Varying amounts of shoreline change were measured along the coast (figs. 8 and 9; table 5). Galveston Island shoreline had the largest average advance (12.2 m), with notable areas of advance near the Bolivar Roads south jetty and along much of West Beach except near San Luis Pass. Average advance between 5 and 10 m was measured along the Brazos/Colorado headland (including Follets Island), Matagorda Peninsula, Matagorda Island, San José Island, and North and South Padre Island. Bolivar Peninsula shoreline also advanced an average of 4.5 m (table 5), with only the segment near the north jetty at Bolivar Roads retreating (fig. 8).

Only two major coastal shoreline segments underwent average shoreline retreat between 2010 and 2011. These included the upper Texas coast between Sabine Pass and High Island (aver-

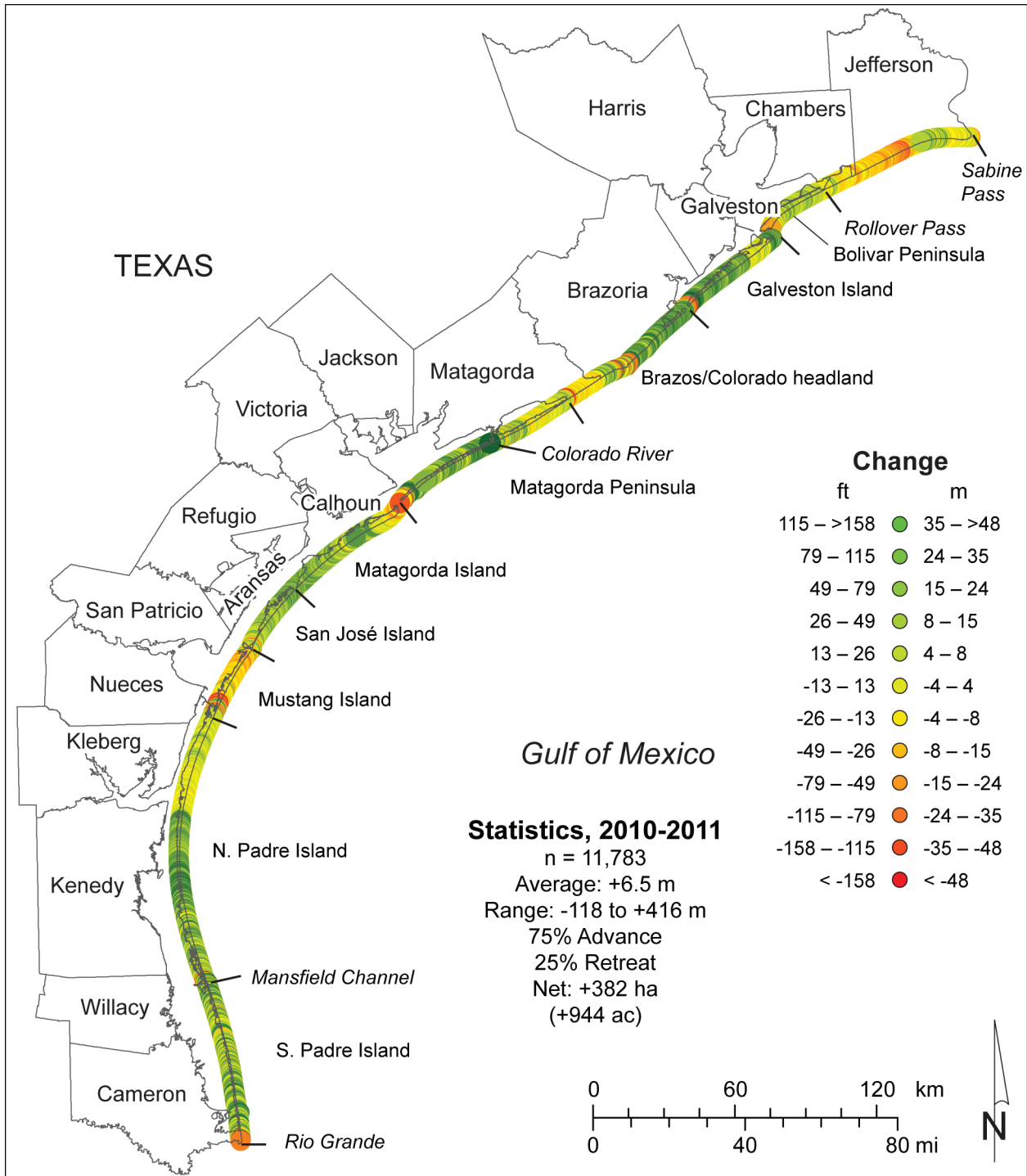


Figure 8. Net shoreline change between April 2010 and April 2011 from Sabine Pass to the Rio Grande. Change calculated from shoreline positions determined from airborne lidar surveys. Positive values indicate shoreline advance; negative values indicate shoreline retreat.

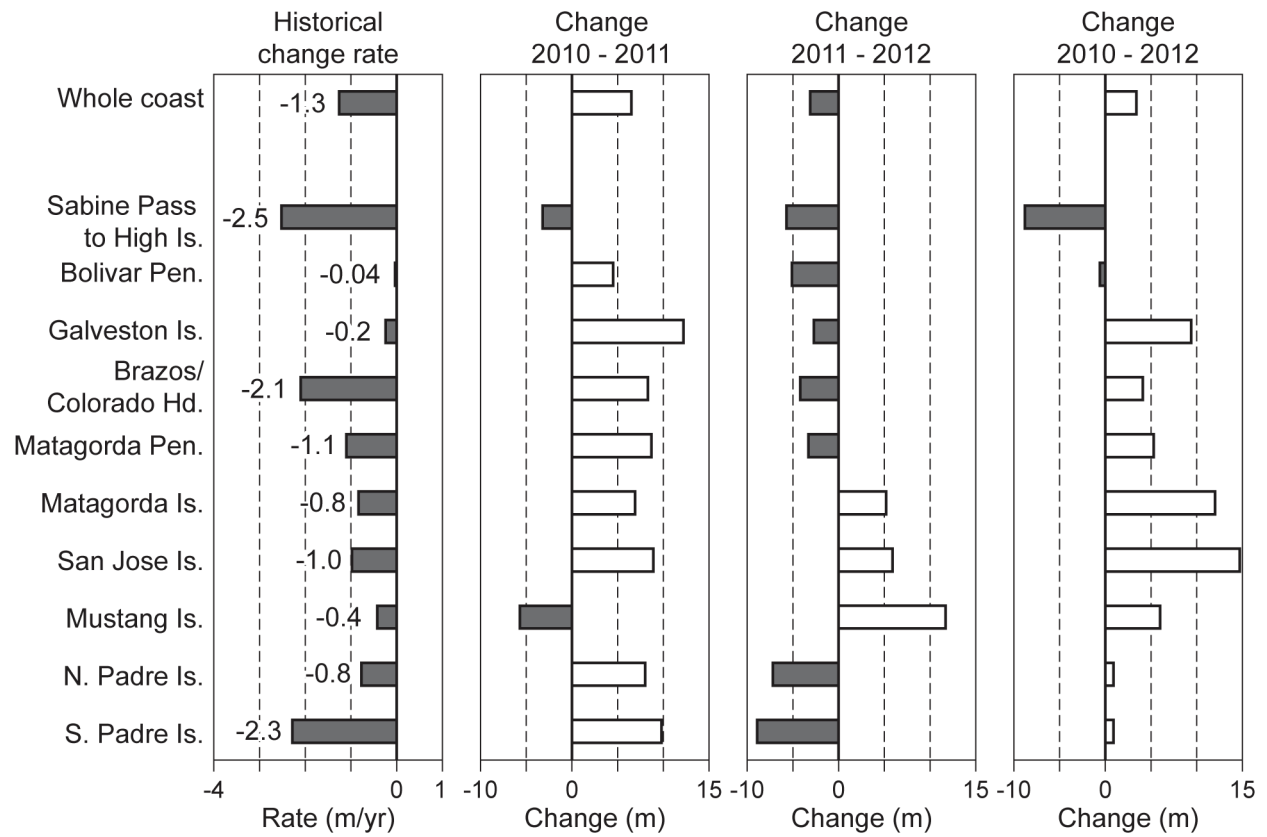


Figure 9. Comparison of incremental shoreline change measured between 2010 and 2012 with long-term shoreline change along the Texas Gulf shoreline.

Table 5. Net shoreline change determined from shoreline position extracted from airborne lidar data acquired in April 2010 and April 2011.

Area	No.	Net change (m)	Std. Dev. (m)	Range (m)	Land area change (ha)
All Texas sites	11,783	6.5	12.3	-118 to 416	+382.1
Upper coast (Sabine Pass to Bolivar Roads)	1894	-0.9	8.2	-110 to 40	-8.7
Upper middle coast (Bolivar Roads to Pass Cavallo)	3777	9.4	15.0	-118 to 416	+177.0
Lower middle coast (Pass Cavallo to Packery Channel)	2329	4.4	9.5	-81 to 55	51.5
Lower coast (Packery Channel to Rio Grande)	3755	8.7	10.5	-82 to 175	+162.9
Sabine Pass to High Island	1337	-3.2	7.6	-29 to 40	-21.2
Bolivar Peninsula	557	4.5	7.1	-110 to 31	+12.5
Galveston Island	937	12.2	20.7	-118 to 416	+57.0
Brazos/Colorado headland	1252	8.3	13.2	-58 to 124	+52.2
Matagorda Peninsula	1582	8.7	11.3	-49 to 84	+68.8
Matagorda Island	1152	6.9	7.1	-19 to 55	+39.5
San Jose Island	627	8.9	5.0	-10 to 25	+27.8
Mustang Island	575	-5.7	10.1	-81 to 19	-16.4
N. Padre Island	2399	8.0	11.4	-82 to 175	+96.5
S. Padre Island	1356	9.8	8.8	-44 to 44	+66.4

age retreat of 3.2 m, table 5) along the historically erosional stretch of low marsh, and Mustang Island (average retreat of 5.7 m) along the historically minimally erosional central Texas coast.

Widespread shoreline advance measured between April 2010 and April 2011 generally counters the long-term trend of shoreline retreat along the entire Texas coast (figs. 7, 8, and 9). Notable segments of advancing shorelines included the area between the Galveston seawall and the Brazos River, Matagorda Peninsula from the Colorado River to the Matagorda Ship Channel, most of Matagorda Island and San José Island, and Padre Island from near Baffin Bay to the southern tip of the island (fig. 8). Significant retreat was limited to the upper coast from near Sabine Pass to High Island, the southern flank of the Brazos/Colorado headland and the eastern part of Matagorda Peninsula, the western end of Matagorda Peninsula and the eastern end of Matagorda Island at Pass Cavallo, Mustang and North Padre Island between Aransas Pass and Baffin Bay, and the shoreline near the mouth of the Rio Grande (fig. 8). Predominant coastwide advance during this period may be attributable to continued recovery from Hurricane Ike during the recovery period from 1.5 to 2.5 years after landfall in September 2008.

Incremental Change between 2011 and 2012

Between the April 2011 and February 2012 airborne surveys, Texas Gulf shorelines predominantly returned to the long-term retreating trend (figs. 7, 9, and 10). Shoreline change measured at 11,811 sites along the coast averaged 3.1 m of retreat; the shoreline retreated at 67 percent of measurement sites. There was a net loss of 181 ha of beach area between April 2011 and February 2012.

With the exception of the central Texas coast, shorelines retreated in all major segments. The largest amount of retreat occurred on Padre Island, where average retreat was 7.2 m on North Padre Island and 8.9 m on South Padre Island (figs. 9 and 10; table 6). Amounts of retreat also generally increased northward from the central to northeastern part of the coast, where retreat increased from an average of 3.3 m on Matagorda Peninsula to 5.7 m on the upper coast between

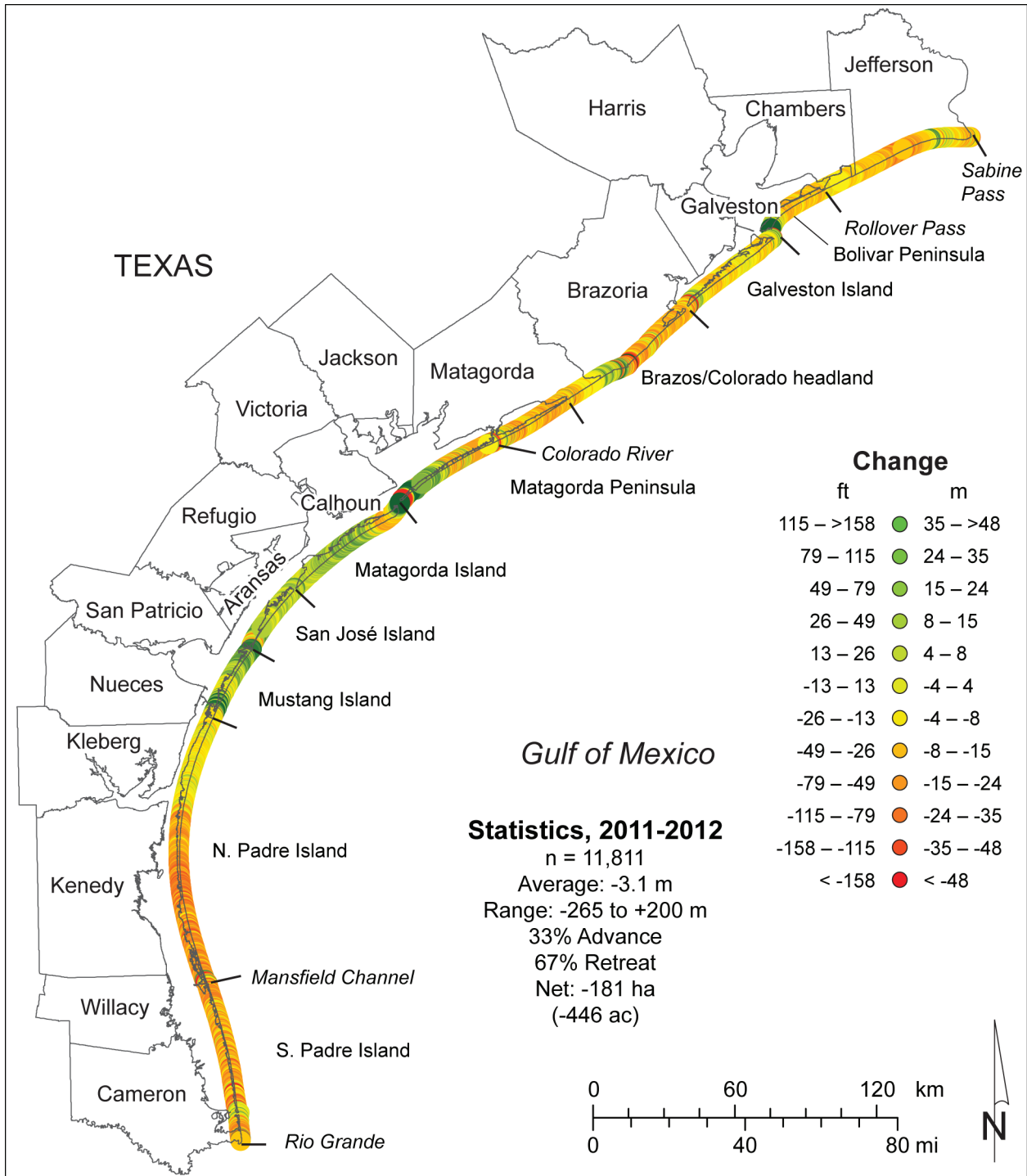


Figure 10. Net shoreline change between April 2011 and February 2012 from Sabine Pass to the Rio Grande. Change calculated from shoreline positions determined from airborne lidar surveys. Positive values indicate shoreline advance; negative values indicate shoreline retreat.

Table 6. Net shoreline change determined from shoreline position extracted from airborne lidar data acquired in April 2011 and February 2012.

Area	No.	Net change (m)	Std. Dev. (m)	Range (m)	Land area change (ha)
All Texas sites	11,811	-3.1	14.3	-265 to 200	-180.5
Upper coast (Sabine Pass to Bolivar Roads)	1899	-5.5	7.3	-123 to 58	-52.1
Upper middle coast (Bolivar Roads to Pass Cavallo)	3798	-3.4	18.6	-265 to 200	-63.8
Lower middle coast (Pass Cavallo to Packery Channel)	2329	6.9	9.0	-16 to 121	+80.3
Lower coast (Packery Channel to Rio Grande)	3757	-7.8	11.3	-173 to 109	-166.6
Sabine Pass to High Island	1342	-5.7	6.4	-41 to 30	-38.0
Bolivar Peninsula	557	-5.1	9.0	-123 to 58	-14.2
Galveston Island	938	-2.7	14.0	-151 to 140	-12.9
Brazos/Colorado headland	1257	-4.2	14.2	-123 to 200	-26.2
Matagorda Peninsula	1596	-3.3	23.1	-265 to 79	-26.5
Matagorda Island	1152	5.2	7.2	-15 to 31	+29.7
San Jose Island	627	5.9	6.2	-16 to 26	+18.4
Mustang Island	575	11.7	12.3	-9 to 121	+33.6
N. Padre Island	2399	-7.2	12.7	-174 to 109	-86.0
S. Padre Island	1358	-8.9	8.3	-48 to 25	-60.7

High Island and Sabine Pass. Average retreat on Galveston Island was 2.7 m, slightly less than adjacent segments to the northeast and southwest of the island. Central coast shorelines advanced average distances that increased southward: 5.2 m on Matagorda Island, 5.9 m on San José Island, and 11.7 m on Mustang Island.

Relative trends in coastwide shoreline change between 2011 and 2012 are similar to long-term patterns (fig. 9). Shorelines along the central coast that advanced between 2011 and 2012 coincide with the area that has among the lowest long-term erosion rates (retreat at 0.4 to 1.0 m/yr on Matagorda Island, San José Island, and Mustang Island, fig. 9). The southward increase in average retreat along Padre Island between 2011 and 2012 coincides with a similar southward increase in long-term retreat rates from North Padre Island (0.8 m/yr) to South Padre Island (2.3 m/yr). Similarly, the northward increase in average shoreline retreat northeastward from Matagorda Peninsula between 2011 and 2012 mirrors the general northeastward increase in long-term retreat rates (excluding Galveston Island and Bolivar Peninsula) to Sabine Pass. Predominance of shoreline retreat along most of the Texas coast between April 2011 and February 2012 may indicate the end of significant recovery from Hurricane Ike and a return to longer-term shoreline change patterns.

Net Change between 2010 and 2012

Predominant retreat along 67 percent of the Texas Gulf shoreline between 2011 and 2012 was insufficient to fully offset advance along 75 percent of the shoreline between 2010 and 2011. As a result, shoreline position in February 2012 was seaward of its position in April 2010 at 59 percent of the 11,811 measurement sites along the coast (fig. 11). The average movement was 3.4 m seaward (fig. 11 and table 7), resulting in a net gain in beach area of 203 ha between 2010 and 2012.

Shorelines along the central coast (Matagorda Island and San José Island) and Galveston Island advanced on average about 10 to 15 m (fig. 9 and table 7). Shorelines to the northeast and south-

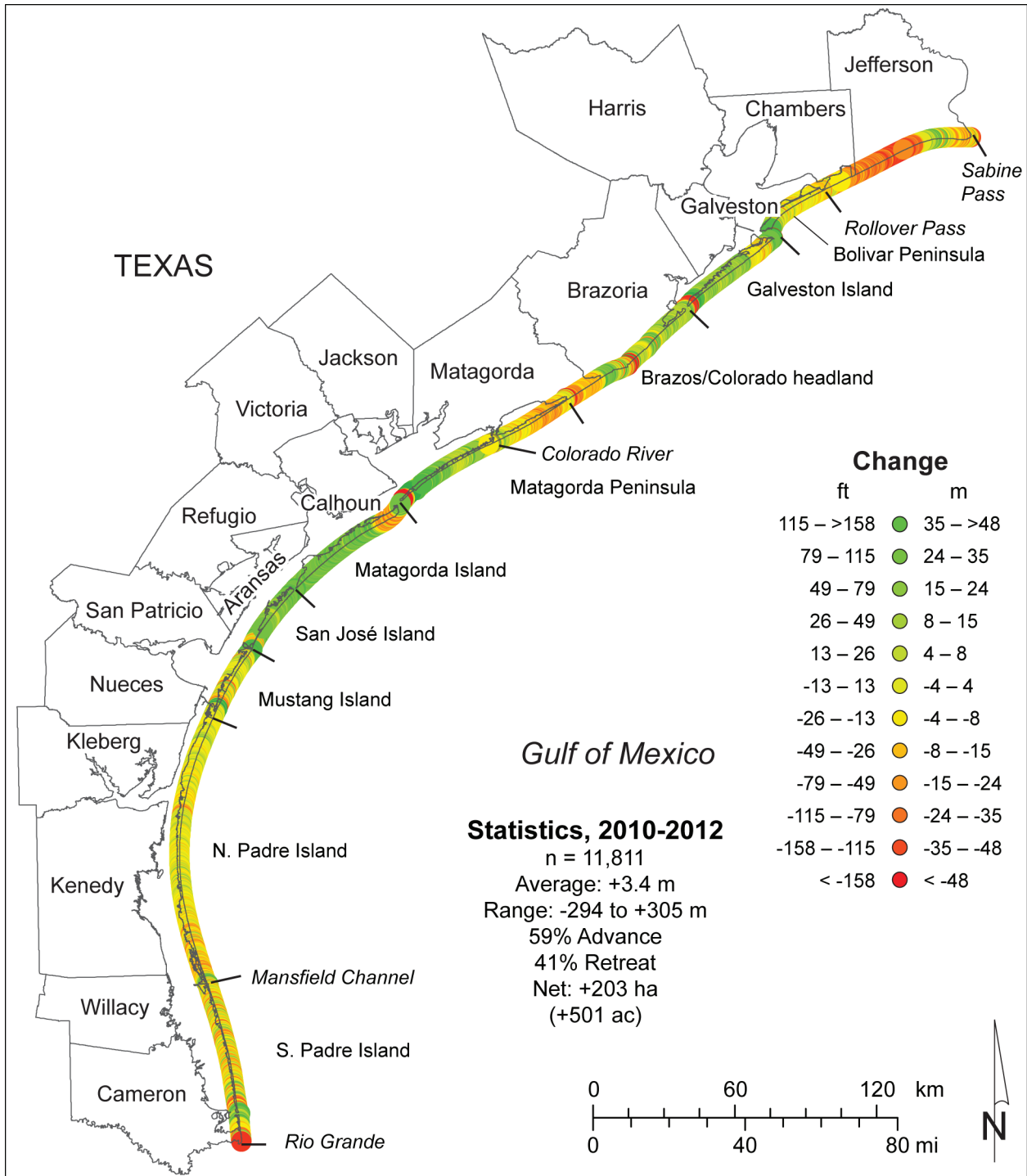


Figure 11. Net shoreline change between April 2010 and February 2012 from Sabine Pass to the Rio Grande. Change calculated from shoreline positions determined from airborne lidar surveys. Positive values indicate shoreline advance; negative values indicate shoreline retreat.

Table 7. Net shoreline change determined from shoreline position extracted from airborne lidar data acquired in April 2010 and February 2012.

Area	No.	Net change (m)	Std. Dev. (m)	Range (m)	Land area change (ha)
All Texas sites	11,811	3.4	16.0	-294 to 305	+202.6
Upper coast (Sabine Pass to Bolivar Roads)	1899	-6.4	11.8	-138 to 40	-60.6
Upper middle coast (Bolivar Roads to Pass Cavallo)	3798	6.0	22.2	-294 to 305	+113.8
Lower middle coast (Pass Cavallo to Packery Channel)	2329	11.3	10.8	-34 to 61	+131.8
Lower coast (Packery Channel to Rio Grande)	3757	0.9	8.0	-25 to 73	+16.5
Sabine Pass to High Island	1342	-8.8	11.6	-44 to 40	-59.0
Bolivar Peninsula	557	-0.6	10.1	-138 to 26	-1.6
Galveston Island	938	9.4	19.2	-124 to 305	+44.1
Brazos/Colorado headland	1257	4.1	17.8	-151 to 233	+26.0
Matagorda Peninsula	1596	5.3	26.4	-294 to 84	+42.5
Matagorda Island	1152	12.0	10.5	-17 to 61	+69.2
San Jose Island	627	14.7	7.3	-10 to 32	+46.2
Mustang Island	575	6.0	12.4	-34 to 41	+17.2
N. Padre Island	2399	0.9	7.1	-20 to 73	+10.5
S. Padre Island	1358	0.9	9.4	-25 to 36	+6.0

west of the advancing central coast also advanced, but over smaller distances (about 5 m along Matagorda Peninsula and the Brazos/Colorado headland to the northeast and Mustang Island to the southwest). Small amounts of average advance or retreat (1 m or less) were measured along Bolivar Peninsula and Padre Island (fig. 9 and table 7). Significant average retreat was measured only along the upper Texas coast between Sabine Pass and High Island (9 m, table 7), the only major segment of the Texas coast where average retreat was measured for both 2010 to 2011 and 2011 to 2012 (fig. 9). Conversely, the most significant shoreline advance for 2010 to 2012 was measured along two central Texas coast barrier islands (Matagorda Island and San José Island), the only segments where average shoreline advance was measured in both periods (2010 to 2011 and 2011 to 2012).

Although short-term net coastwide trends measured from 2010 to 2012 generally show shoreline advance, the relative rates of advance are similar to the long-term shoreline change patterns. The greatest amount of shoreline advance between 2010 and 2012 was measured along the central coast between Matagorda Peninsula and Mustang Island, coincident with the segment of the Texas coast where long-term average retreat rates are relatively low (0.4 to 1.1 m/yr, fig. 9). The greatest amount of shoreline retreat between 2010 and 2012 occurred on the upper coast between Sabine Pass and High Island, where the most rapid long-term average retreat rates have been measured (2.5 m/yr). Small average amounts of shoreline advance were measured along Padre Island, where long-term patterns indicate moderate to high average rates of erosion.

ELEVATION-THRESHOLD AREAS

Extracting a chosen elevation contour from the DEM and using it as a proxy for shoreline position is a convenient way to examine shoreline position and movement over time, but much more information is available from a DEM that covers the beach and dune system. In particular, the DEM can be “sliced” at arbitrary elevations, readily yielding the area that is at or above that threshold elevation. Beginning with the 2-m msl elevation threshold, we have calculated the total area within the survey swath and within each coastal county that exceeds the chosen threshold el-

evation. We then increased the elevation at 1-m increments to a maximum elevation of 9 m msl, calculating total areas exceeding each threshold elevation. Plotting threshold elevation against area exceeding that elevation for each segment of the Texas Gulf shoreline produces elevation-threshold area, or ETA, curves that reveal several important attributes related to coastal landform morphology. These include (1) susceptibility to storm surge and flooding at arbitrary surge heights, (2) sand storage within the beach and dune system, (3) maturity and extent of dunes, and (4) resistance and recoverability from chronic and instantaneous erosion events. ETA curves also provide a rapid framework in which to monitor area and volume change over time, which in turn enables a more complete understanding of beach and dune system change.

At the Bureau, we determined ETA curves for the entire coast for the April 2010, April 2011, and February 2012 airborne surveys (fig. 12). These curves, determined over a 300- to 500-m-wide swath along the Gulf shoreline, reveal a rapid reduction in total area as threshold elevations are increased. At 2-m msl, for example, the coastal swath encompasses 66 (in 2012) to 77 (in 2010) km² of area at or above that elevation. Above the 3-m threshold, less than half that area (31 to 34 km², depending on the year) is at or above that elevation. The reduction in surface area by approximately half with each 1-m increase in threshold elevation holds throughout the elevation range. At the highest threshold elevation of 9 m, there is less than 1 km² of area within the lidar swath that exceeds that elevation.

ETA curves can be constructed for any area. To illustrate some of the differences in morphology evident along the Texas coast, we have calculated ETAs for each coastal county (Appendix A) and have grouped them into upper, middle, and lower coast curves (fig. 13) using 2012 airborne survey data. To standardize the comparison among counties with differing shoreline lengths, the county ETA curves have been normalized by dividing the threshold areas by the shoreline length in each county.

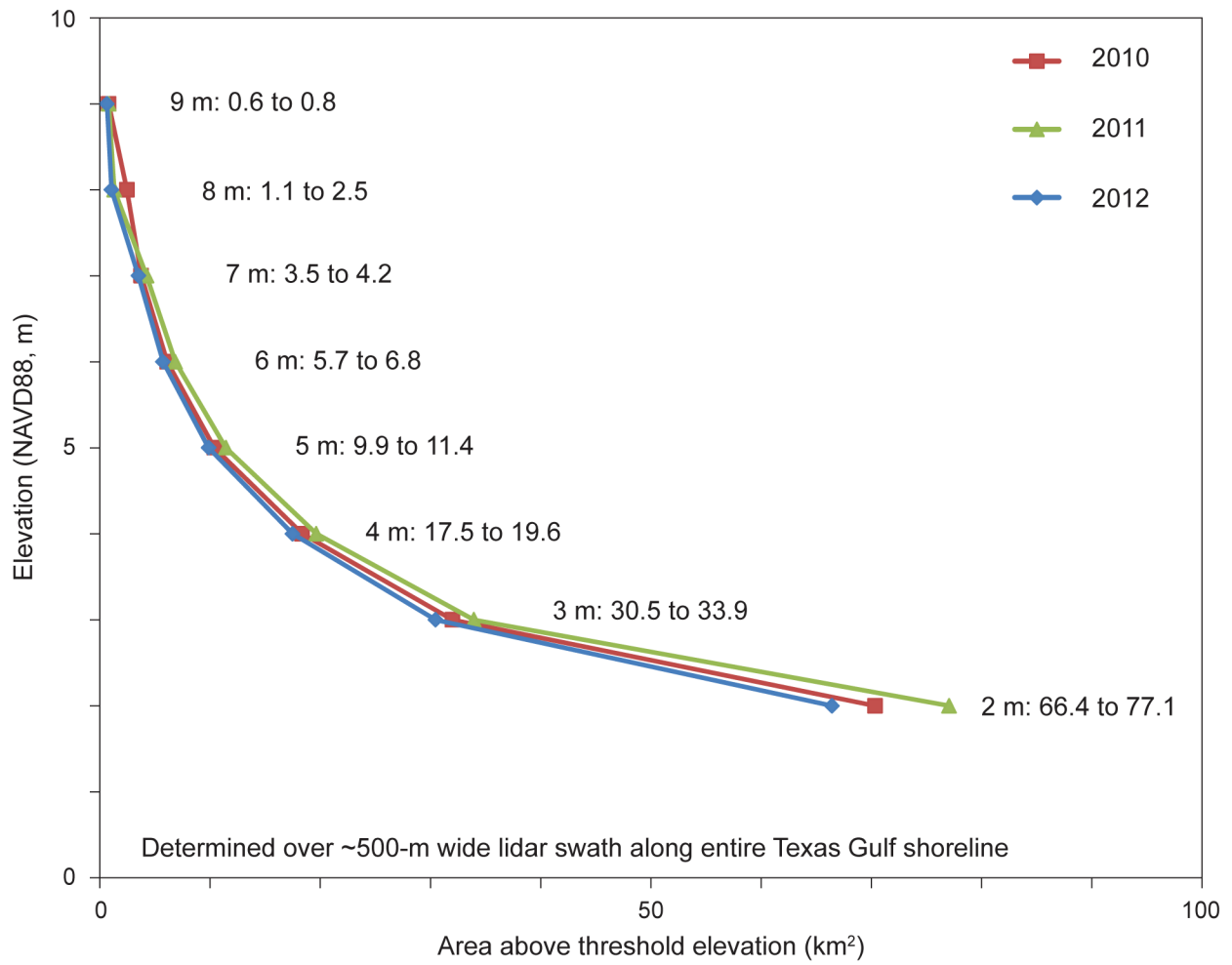


Figure 12. Total area above threshold elevations in 2010, 2011, and 2012 along the Texas Gulf shoreline.

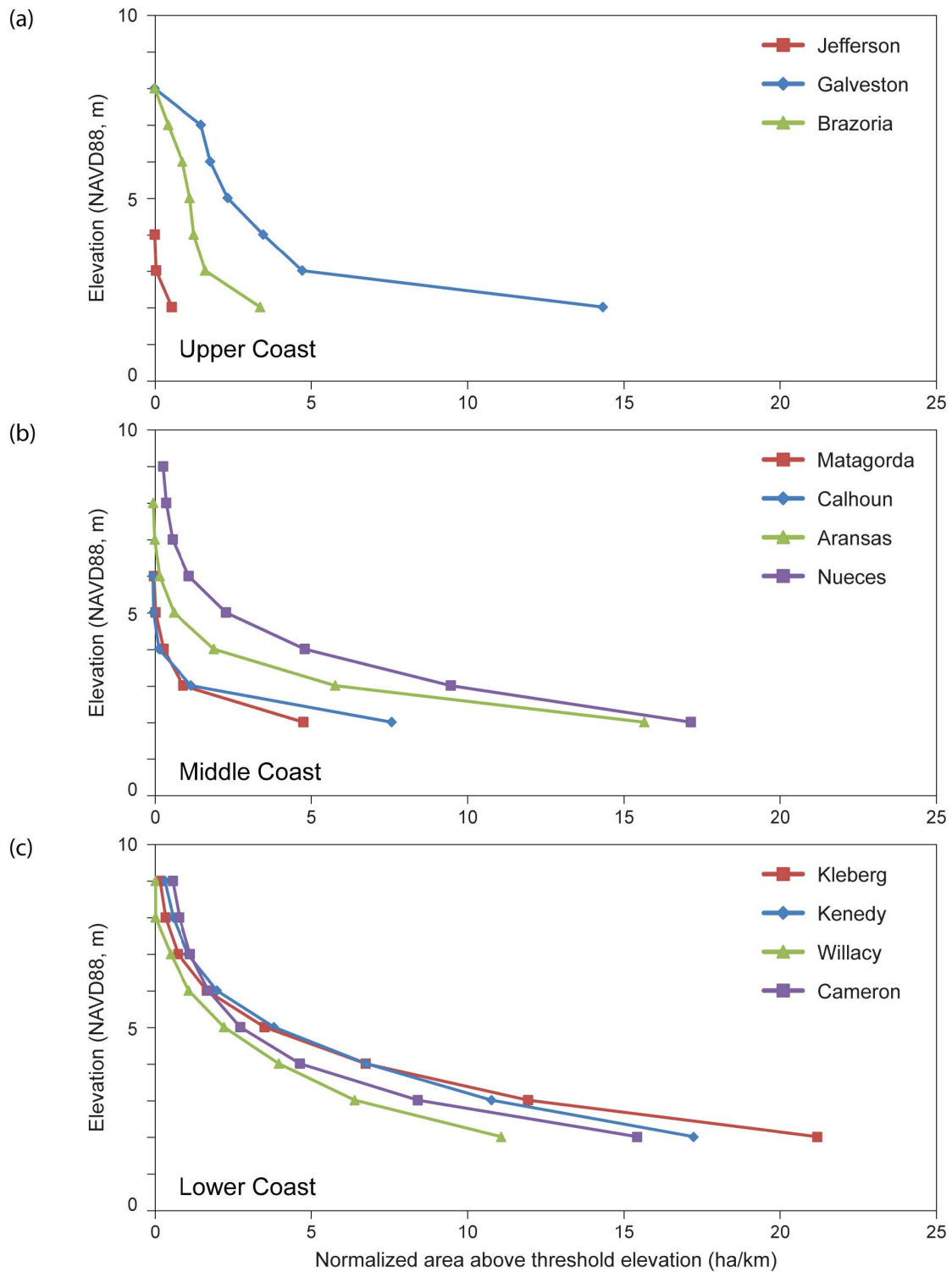


Figure 13. Normalized area above threshold elevations for upper, middle, and lower coast counties, Texas Gulf coast. ETA curves calculated from 2012 lidar-derived DEMs. Areas are normalized by dividing the total area above a given threshold elevation in a county by the length of shoreline in the county.

Upper Coast

Upper coast ETA curves include those for Jefferson (including Chambers), Galveston, and Brazoria counties, extending from Sabine Pass to near the mouth of the Brazos River (fig. 1). Shorelines along Jefferson County are the most rapidly retreating in Texas. The ETA curve for Jefferson County has the smallest area above threshold elevation for any Texas coastal county, along with the lowest elevation above which virtually no area above that elevation exists within the lidar survey swath (4 m msl, fig. 13a and Appendix A). At Sea Rim State Park (fig. 14), for example, the lidar-derived DEM along the shoreline (fig. 14b) shows numerous erosional features and the generally low elevation (mostly less than 3 m) of the area. Area slices at threshold elevations of 2 m (fig. 14c) and 3 m (fig. 14d) show how little of the land surface exceeds those elevations. The ETA curve readily reveals that this area is highly susceptible to flooding even at low to moderate storm surge heights, sand storage in the beach and dune system is minimal, and the area is highly susceptible to chronic and instantaneous erosion.

ETA curves for other upper coast counties (Galveston and Brazoria, including Bolivar Peninsula, Galveston Island, Follets Island, and the northeastern part of the Brazos/Colorado headland) each show considerably more area above each threshold elevation (fig. 13a). Maximum threshold elevation for these counties is about 8 m, above which little area remains. Galveston County includes about twice as much area above a given threshold elevation as does Brazoria County, but a significant fraction of the area at higher threshold elevations is located along the seawall.

Middle Coast

Middle coast ETA curves include those for Matagorda (including the Brazos/Colorado headland and Matagorda Peninsula), Calhoun (Matagorda Island), Aransas (San José Island), and Nueces (Mustang Island) counties. These areas are within the least erosional part of the Texas coast, where average rates of long-term shoreline retreat range from 0.4 to 1.1 m/yr (fig. 9). ETA curves for these counties are progressively higher and wider from north to south, following the trend of southward-decreasing retreat rates. Matagorda, the northernmost county, has the low-

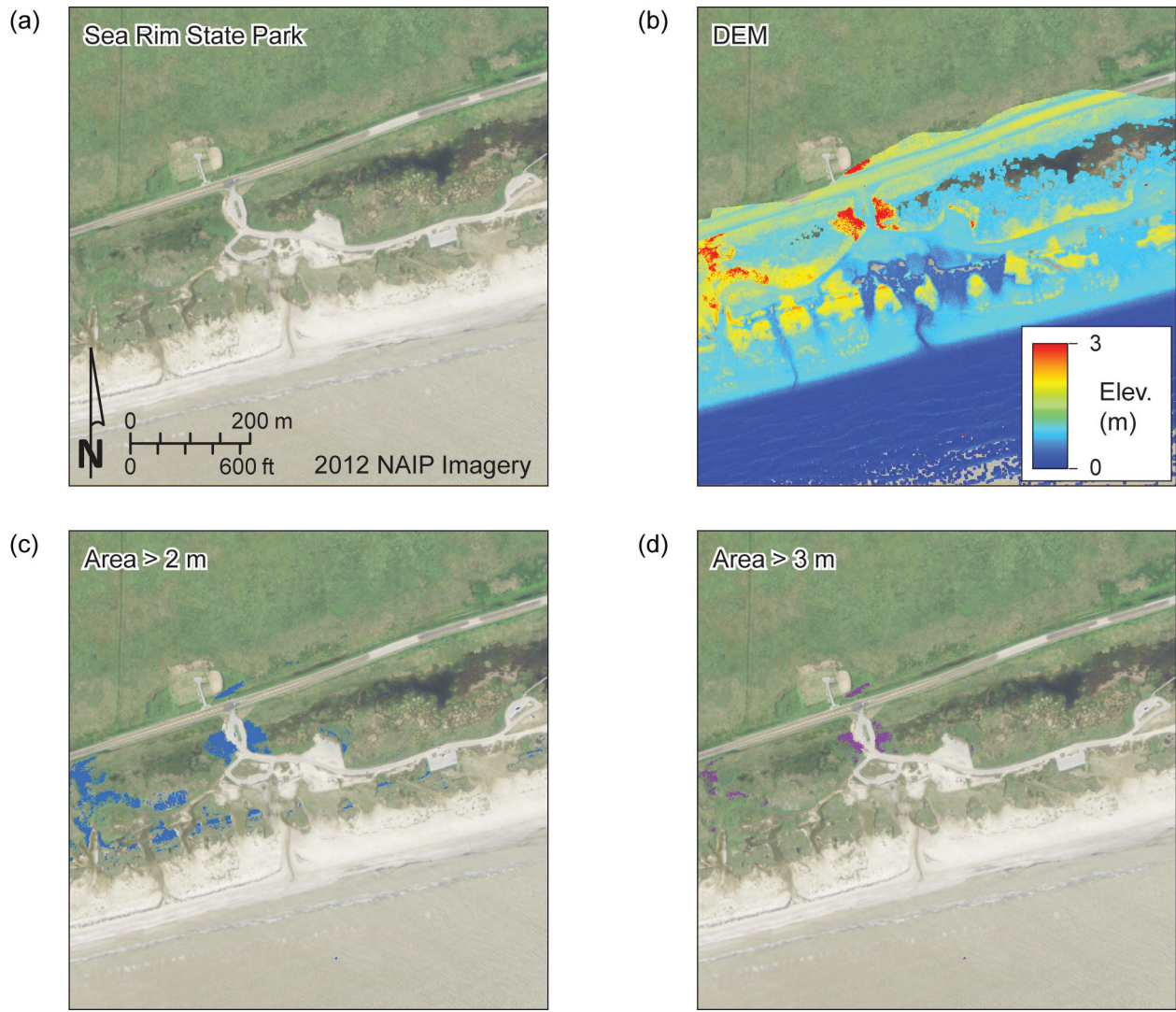


Figure 14. Sea Rim State Park DEM (b) and area slices at threshold elevations of (c) 2 m and (d) 3 m.

est maximum elevation threshold at about 5 m (similar to Calhoun County), and also has the lowest normalized area above threshold elevations of the four middle coast counties (fig. 13b). Calhoun County, encompassing most of Matagorda Island, has a similar curve, but has slightly higher areas at threshold elevations of 2 and 3 m. A DEM and series of elevation slices along the shore at a site on Matagorda Island (fig. 15) demonstrates the difference in morphology between a more stable middle coast setting and the highly erosional upper coast site at Sea Rim State Park (fig. 14). The DEM on Matagorda Island shows prominent ridge-and-swale topography that reaches maximum elevations of about 7 m msl (fig. 15b). Slices through the DEM at 2 m, 3 m, 4 m, and 5 m (fig. 15c, d, e, f) show large areas exceeding lower threshold elevations, along with more limited areas exceeding higher threshold areas farther onshore on the mature dune crests.

Farther south along the middle coast, Aransas County (encompassing San José Island) has a significantly higher maximum threshold elevation of about 8 m than areas farther to the northeast. It also has areas above threshold elevations of 2 through 6 m that considerably exceed those for the Brazos/Colorado headland, Matagorda Peninsula, and Matagorda Island. The most robust ETA curves are found farther to the southwest in Nueces County (Mustang Island), where the maximum threshold elevation exceeds 9 m and areas above threshold elevations are the highest of any middle coast county (fig. 13b).

Lower Coast

The lower coast counties (Kleberg, Kenedy, Willacy, and Cameron) cover most of Padre Island. Average rates of long-term shoreline retreat generally increase southward along this coastal segment, increasing from 0.8 m/yr on North Padre Island to 2.3 m/yr on South Padre Island (fig. 9). ETA curves for all counties on Padre Island have relatively high maximum threshold elevations of 9 m or more (fig. 13c), but those in the southernmost county (Cameron) on South Padre Island are skewed at the higher elevations by the presence of structures within the lidar swath. Near the convention center on South Padre Island, for example, the lidar-derived DEM has a maximum elevation exceeding 10 m (fig. 16b), showing the presence of high, mature dunes as well as rect-

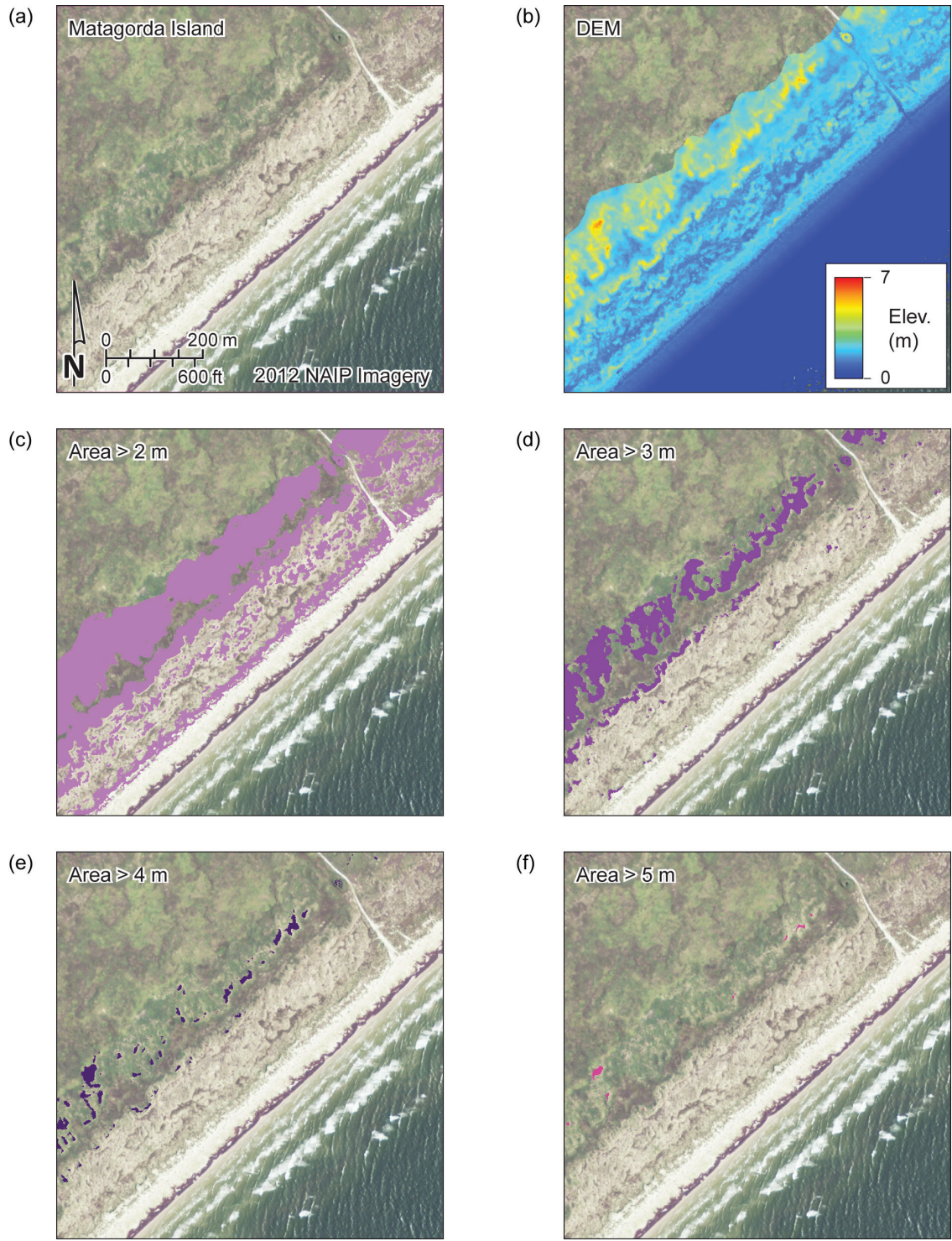


Figure 15. Matagorda Island DEM (b) and area slices at threshold elevations of (c) 2 m, (d) 3 m, (e) 4 m, and (f) 5 m.

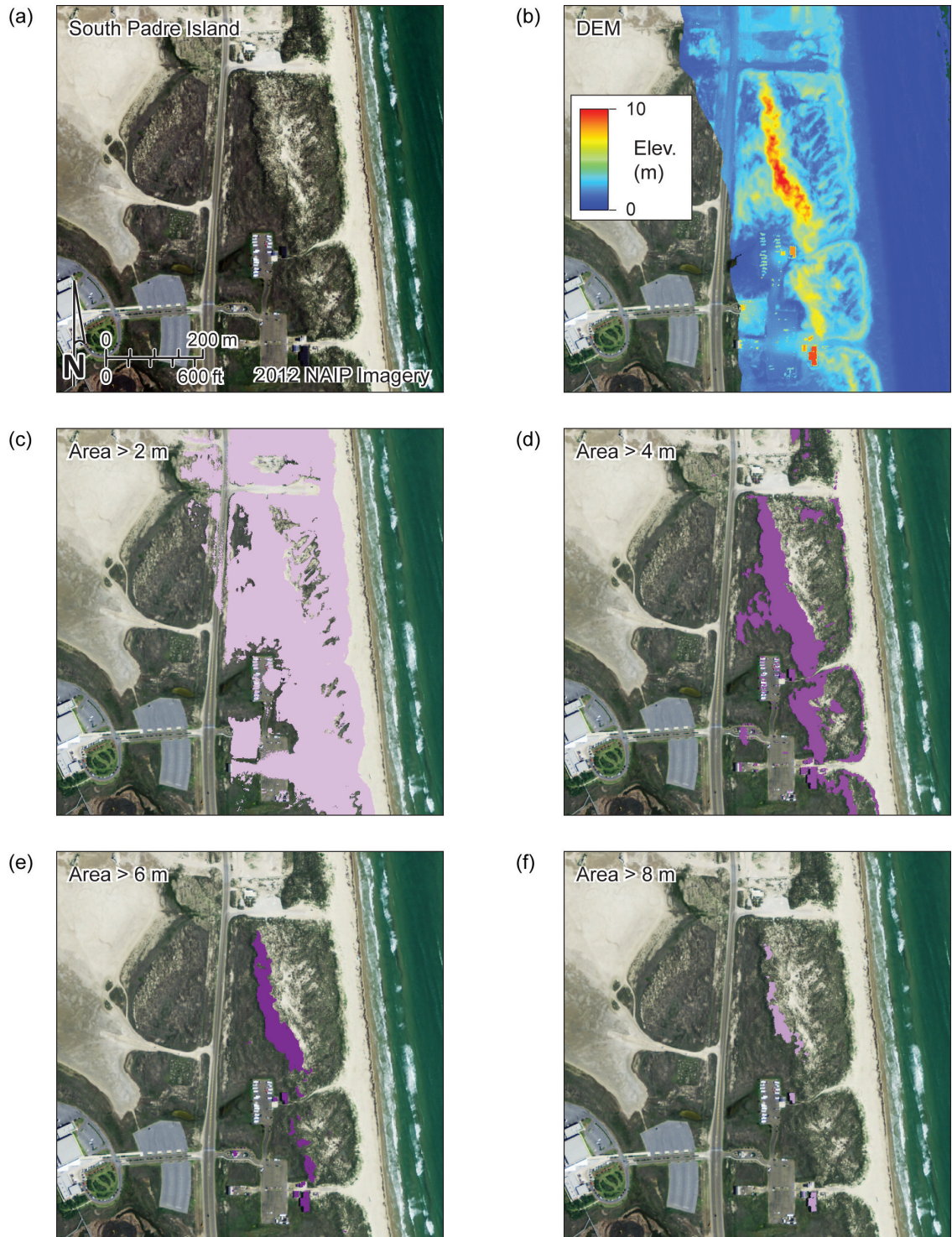


Figure 16. South Padre Island DEM (b) and area slices at threshold elevations of (c) 2 m, (d) 4 m, (e) 6 m, and (f) 8 m.

angular buildings. Elevation slices through the DEM at 2 m, 4 m, 6 m, and 8 m (fig. 16c, d, e, f) show progressively decreasing areas exceeding those elevations. At the highest elevation shown (8 m), only the crest of a high, mature dune and nearby buildings remain.

ETA curves for the southern part of Padre Island (Cameron and Willacy county) are similar to those for the northern part of Padre Island at the higher elevation thresholds (6 m and higher), but have significantly lower areas at threshold elevations of 2 to 5 m. This suggests that sand storage and erosion resilience are greater along the central and northern parts of Padre Island (in Kleberg and Kenedy counties) than they are on the southern part of the island (Willacy and Cameron counties).

STORM SUSCEPTIBILITY INDEX

The Storm Susceptibility Index (SSI) is a tool that helps assess the potential level of upland protection that beaches and dunes could provide against surge and erosion resulting from a tropical storm or hurricane. This index (table 8), combined with information on priority areas for protection, can be used to help determine needs for projects to mitigate future storm damage. Results from the SBEACH simulations (Appendix C) as well as measurements of the different beach and dune characteristics were used by HRI to create an eight-level index that describes the susceptibility of a given location to overwash during a storm event.

Table 8. Eight protection levels of the Storm Susceptibility Index.

Protection level	Description
1	Protection against a 1-year storm or less
2	Protection against a 2-year storm or less
3	Protection against a 5-year storm or less
4	Protection against a 10-year storm or less
5	Protection against a 20-year storm or less
6	Protection against a 50-year storm or less
7	Protection against a 100-year storm or less
8	Protection against a 200-year storm or less

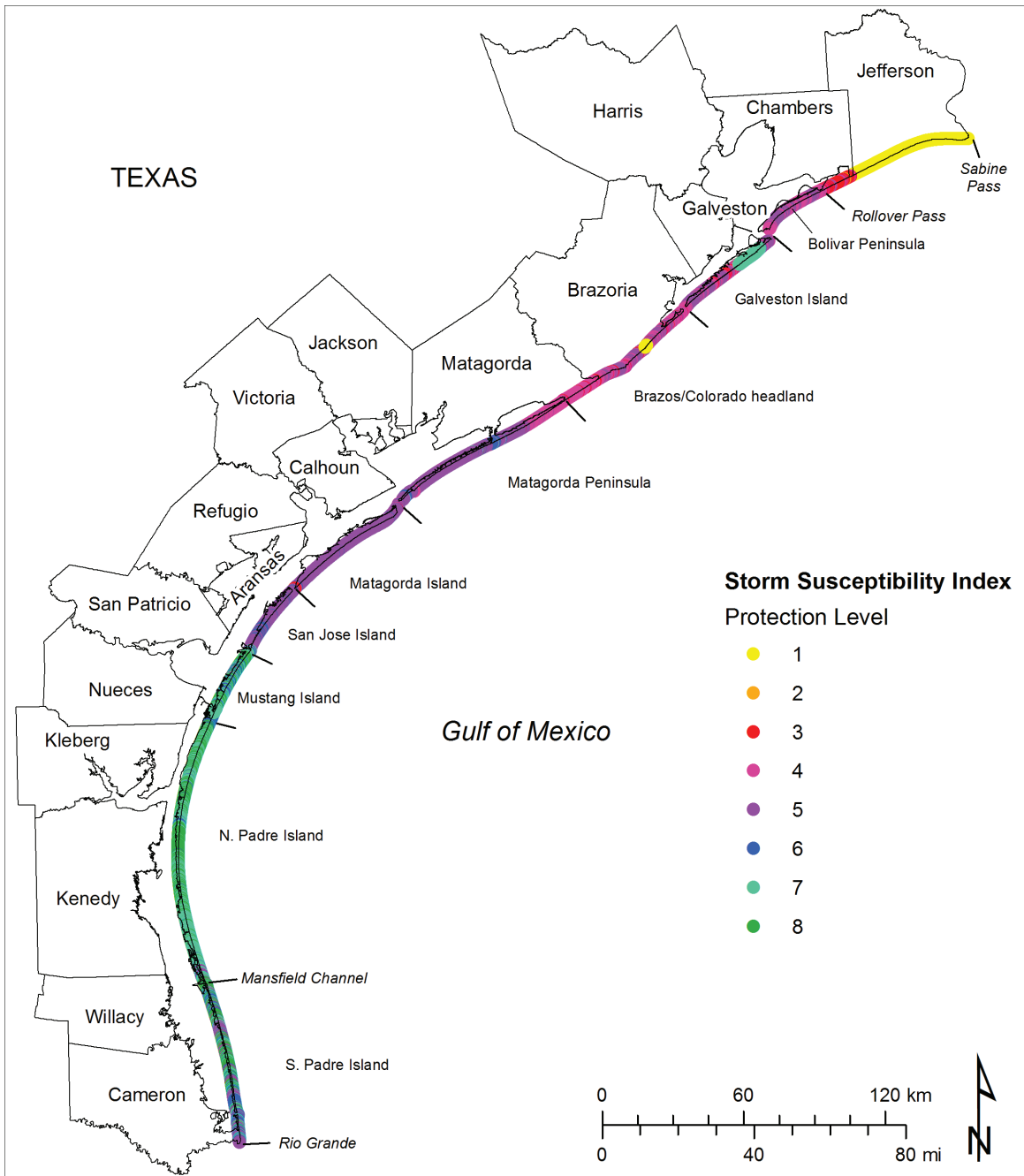


Figure 17. Storm Susceptibility Index protection levels determined for the Texas coast. Lowest storm susceptibility levels (protection against a 1-year storm or less) are found along all of Jefferson County on the upper Texas coast. Shorelines with the highest storm susceptibility levels (protection against a 200-year storm) are found on North Padre Island. Data from HRI.

The lowest level of storm protection (SSI level 1) is found along the upper Texas coast, particularly in Jefferson County (fig. 17). ETA curves constructed from lidar-derived DEMs indicate that the beach and dune system in this area has generally low elevation and provides minimal protection from even the smallest storm (figs. 13a and 14). The middle Texas coast (Matagorda Peninsula, Matagorda Island, and San José Island) Storm Susceptibility Index ranges between levels 4 (10-year storm) and 6 (50-year storm, table 8), a relationship that is consistent with middle coast ETA curves (figs. 13b and 15). Storm protection levels increase with increasing areas with threshold elevations above 2 to 3 m. The large foredunes on Mustang Island and Padre Island offer the highest levels of protection. Storm susceptibility protection decreases towards the southern extent of South Padre Island in the developed area of the barrier island.

CONCLUSIONS

Three annual airborne lidar surveys of the Texas Gulf shoreline were acquired in 2010, 2011, and 2012. High-resolution digital elevation models (DEMs) constructed from the lidar data allowed extraction of critical coastal features (including the shoreline, potential vegetation line, and landward dune boundary). Short-term shoreline change was determined by comparing annual extracted shoreline position, indicating that shorelines predominantly advanced between 2010 and 2011 during ongoing recovery from Hurricane Ike (2008) and retreated between 2011 and 2012. The more recent trends are similar to long-term shoreline change trends that indicate all major segments of the Texas Gulf shoreline are retreating at a coastwide average rate of about 1.2 m/yr. Between 2010 and 2012, the Texas Gulf shoreline advanced at 59 percent of measurement sites over an average distance of 3.4 m, resulting in a net beach-area gain of 203 ha.

DEMs were used to examine beach and dune land areas above threshold elevations ranging from 2 to 9 m msl. These elevation-threshold area (ETA) curves are readily determined from DEMs and are useful in assessing sand storage, storm surge flooding susceptibility, and erosion susceptibility and recovery potential. ETA curve patterns for principal coastal geomorphic units and coastal counties correlate well with long-term shoreline change rates; areas with high threshold

elevations and large threshold-elevation areas are found in relatively stable areas of the Texas coast, whereas areas with low threshold elevations and limited threshold-elevation areas are found in areas such as the upper Texas coast where the highest long-term retreat rates and frequent surge inundation occur.

DEMS constructed from lidar data enabled development of a storm susceptibility index (SSI) for the Texas Gulf shoreline that includes 8 levels of protection from storms with recurrence intervals of 1 year (level 1) to 200 years (level 8).

ACKNOWLEDGMENTS

This project was supported by grant no. 09-242-000-3789 from the General Land Office of Texas to the Bureau of Economic Geology, The University of Texas at Austin. Jeffrey G. Paine served as the principal investigator. This project was funded by a financial assistance award from the U.S. Department of the Interior, U.S. Fish and Wildlife Service, Coastal Impact Assistance Program. Bureau staff Aaron Averett, Ruth Costley, and Sojan Mathew assisted with the airborne lidar surveys. Lidar survey support was also provided by Jim Reed, Roy Scott, Bob Rodell, David Morgan, Andre Fuegner, and Leonard Laws (Texas Department of Transportation); Alistair Lord and Greg Hauger (Texas A&M–Corpus Christi); Dan Prouty (National Geodetic Survey); and Roberto Gutierrez (UT Center for Space Research). The views expressed herein are those of the authors and do not necessarily reflect the views of the U. S. Fish and Wildlife Service. Carly Vaughn (General Land Office) served as project manager.

REFERENCES

- Avila, L. A., 2010, Tropical Storm Hermine (AL102010): Tropical Cyclone Report, National Hurricane Center, 17 p.
- Barnett, T. P., 1983, Global sea level: estimating and explaining apparent changes: in Magoon, O. T., and Converse, H., editors, Coastal Zone '83, Proceedings of the Third Symposium on Coastal and Ocean Management, v. 3, p. 2777-2783.
- Bender, C., Smith, J. M., and Kennedy, A., 2010, Hurricane Ike (2008) nearshore waves: simulations and measurements: In Proceedings of the 32nd Conference on Coastal Engineering: Coastal Engineering 2010, Shanghai, China 2010, v. 1, p. 1-12.

- Berg, R., 2009, Hurricane Ike (AL092008): Tropical Cyclone Report, National Hurricane Center, 55 p.
- Brennan, M. J., 2011, Tropical Storm Don (AL042011): Tropical Cyclone Report, National Hurricane Center, 15 p.
- Bruun, P., 1954, Coastal erosion and development of beach profiles: Technical Memorandum, v. 44, Beach Erosion Board, U. S. Army Corps of Engineers, 82 p.
- Bruun, P., 1962, Sea-level rise as a cause of shore erosion: Proceedings, American Society of Civil Engineers, Journal of the Waterways and Harbors Division, v. 88, p. 117-130.
- Bruun, P., 1988, The Bruun rule of erosion by sea-level rise: a discussion of large-scale two- and three-dimensional usages: Journal of Coastal Research, v. 4, p. 627-648.
- Cazenave, A., and Nerem, R. S., 2004, Present-day sea level change: observations and causes: Reviews of Geophysics, v. 42, RG3001, doi: 1029/2003RG000139, 20 p.
- Church, J. A., and White, N. J., 2006, A 20th century acceleration in global sea-level rise: Geophysical Research Letters, v. 33: L01602, doi: 10.1029/2005GL024826.
- Cooper, J. A. G., and Pilkey, O. H., 2004, Sea-level rise and shoreline retreat: time to abandon the Bruun Rule: Global and Planetary Change, v. 43, p. 157-171.
- Emery, K. O., 1980, Relative sea levels from tide-gauge records: Proceedings, National Academy of Sciences, USA, v. 77: p. 6968-6972.
- FitzGerald, D. M., Fenster, M. S., Argow, B. A., and Buynevich, I. V., 2008, Coastal impacts due to sea-Level rise: Annual Review of Earth and Planetary Sciences, v. 36, p. 601-647.
- Gibeaut, J. C., and Caudle, T., 2009, Defining and mapping foredunes, the line of vegetation, and shorelines along the Texas Gulf Coast: Final Report for The Texas General Land Office.
- Gibeaut, J. C., Gutierrez, R., and Hepner, T., 2002, Threshold conditions for episodic beach erosion along the southeast Texas coast: Gulf Coast Association of Geological Societies Transactions, v. 52, p. 323-335.
- Gibeaut, J. C., Hepner, Tiffany, Waldinger, Rachel, Andrews, John, Gutierrez, Roberto, Tremblay, T. A., and Smyth, Rebecca, 2001, Changes in Gulf shoreline position, Mustang and North Padre Islands, Texas: Bureau of Economic Geology, The University of Texas at Austin, Report to the Texas Coastal Coordination Council and the General Land Office, contract no. 00-002r, 29 p.
- Gibeaut, J. C., White, W. A., Hepner, Tiffany, Gutierrez, Roberto, Tremblay, T. A., Smyth, R. A., and Andrews, John, 2000, Texas Shoreline Change Project: Gulf of Mexico shoreline change from the Brazos River to Pass Cavallo: Bureau of Economic Geology, The University of Texas at Austin, Report to the Texas Coastal Coordination Council and the General Land Office, contract no. NA870Z0251, 32 p.
- Gornitz, V., Lebedeff, S., and Hansen, J., 1982, Global sea level trend in the past century: Science, v. 215, p. 1611-1614.
- Gornitz, V., and Lebedeff, S., 1987, Global sea-level changes during the past century: in Nummedal, D., Pilkey, O. H., and Howard, J. D., editors, Sea level fluctuation and coastal

- evolution: Society of Economic Paleontologists and Mineralogists Special Publication 41, p. 3-16.
- Gutenberg, B., 1941, Changes in sea level, postglacial uplift, and mobility of the Earth's interior: Geological Society of America Bulletin, v. 52, p. 721-772.
- Hayes, M. O., 1967, Hurricanes as geological agents: case studies of hurricanes Carla, 1961, and Cindy, 1963: The University of Texas at Austin, Bureau of Economic Geology Report of Investigations No. 61, 54 p.
- King, D. B., 2007, Wave and beach processes modeling for Sabine Pass to Galveston Bay, Texas, Shoreline Erosion Feasibility Study (No. ERDC/CHL TR-07-6): Coastal and Hydraulics Laboratory, U.S. Army Engineer Research and Development Center.
- Leuliette, E. W., and Miller, L., 2009, Closing the sea level rise budget with altimetry, Argo, and GRACE: Geophysical Research Letters, v. 36, L04608, doi:10.1029/2008GL036010.
- Lyles, S. D., Hickman, L. E., Jr., and Debaugh, H. A., Jr., 1988, Sea level variations for the United States, 1855-1986: National Ocean Service, Rockville, Maryland, 182 p.
- Morton, R. A., 1974, Shoreline changes on Galveston Island (Bolivar Roads to San Luis Pass), an analysis of historical changes of the Texas Gulf Shoreline: The University of Texas at Austin, Bureau of Economic Geology Geological Circular 74-2, 34 p.
- Morton, R. A., 1975, Shoreline changes between Sabine Pass and Bolivar Roads: The University of Texas at Austin, Bureau of Economic Geology Geological Circular 75-6, 43 p.
- Morton, R. A., 1977, Historical shoreline changes and their causes, Texas Gulf Coast: Gulf Coast Association of Geological Societies Transactions, v. 27, p. 352-364. Reprinted as Bureau of Economic Geology Geological Circular 77-6, 13 p.
- Morton, R. A., 1997, Gulf shoreline movement between Sabine Pass and the Brazos River, Texas: 1974 to 1996: Bureau of Economic Geology Geological Circular 97-3, 46 p.
- Morton, R. A., Miller, T. L., and Moore, L. J., 2004, National assessment of shoreline change, part 1: historical shoreline changes and associated coastal land loss along the U.S. Gulf of Mexico: U.S. Geological Survey Open-File Report 2004-1043, 42 p.
- Morton, R. A., and Paine, J. G., 1985, Beach and vegetation-line changes at Galveston Island, Texas: erosion, deposition, and recovery from Hurricane Alicia: The University of Texas at Austin, Bureau of Economic Geology Geological Circular 85-5, 39 p.
- Morton, R. A., and Paine, J. G., 1990, Coastal land loss in Texas: an overview: Transactions, Gulf Coast Association of Geological Societies, v. 40, p. 625-634.
- Morton, R. A., Paine, J. G., and Gibeaut, J. C., 1994, Stages and durations of post-storm beach recovery, southeastern Texas coast, U.S.A.: Journal of Coastal Research, v. 10, p. 884-908.
- Morton, R. A., and Pieper, M. J., 1975a, Shoreline changes on Brazos Island and South Padre Island (Mansfield Channel to mouth of the Rio Grande), an analysis of historical changes of the Texas Gulf shoreline: The University of Texas at Austin, Bureau of Economic Geology, Geological Circular 75-2, 39 p.

- Morton, R. A., and Pieper, M. J., 1975b, Shoreline changes in the vicinity of the Brazos River delta (San Luis Pass to Brown Cedar Cut): The University of Texas at Austin, Bureau of Economic Geology Geological Circular 75-4, 47 p.
- Morton, R. A., and Pieper, M. J., 1976, Shoreline changes on Matagorda Island and San Jose Island (Pass Cavallo to Aransas Pass): The University of Texas at Austin, Bureau of Economic Geology Geological Circular 76-4, 42 p.
- Morton, R. A., and Pieper, M. J., 1977a, Shoreline changes on Mustang Island and North Padre Island (Aransas Pass to Yarborough Pass): The University of Texas at Austin, Bureau of Economic Geology Geological Circular 77-1, 45 p.
- Morton, R. A., and Pieper, M. J., 1977b, Shoreline changes on central Padre Island (Yarborough Pass to Mansfield Channel): The University of Texas at Austin, Bureau of Economic Geology Geological Circular 77-2, 35 p.
- Morton, R. A., Pieper, M. J., and McGowen, J. H., 1976, Shoreline changes on Matagorda Peninsula (Brown Cedar Cut to Pass Cavallo): The University of Texas at Austin, Bureau of Economic Geology Geological Circular 76-6, 37 p.
- Paine, J. G., 1991, Late Quaternary depositional units, sea level, and vertical movement along the central Texas coast: Ph. D. dissertation, University of Texas at Austin, Austin, Texas, 256 p.
- Paine, J. G., 1993, Subsidence of the Texas coast: inferences from historical and late Pleistocene sea levels: *Tectonophysics*, v. 222, p. 445–458.
- Paine, J. G., Mathew, S., and Caudle, T., 2011, Texas Gulf shoreline change rates through 2007: Bureau of Economic Geology, The University of Texas at Austin, report prepared under General Land Office contract no. 10-041-000-3737 and National Oceanic and Atmospheric Administration award no. NA09NOS4190165, 38 p. + CD-ROM.
- Paine, J. G., Mathew, Sojan, and Caudle, Tiffany, 2012, Historical shoreline change through 2007, Texas Gulf coast: rates, contributing causes, and Holocene context: *GCAGS Journal*, v. 1, p. 13-26.
- Paine, J. G., and Morton, R. A., 1989, Shoreline and vegetation-line movement, Texas Gulf Coast, 1974 to 1982: The University of Texas at Austin, Bureau of Economic Geology Geological Circular 89-1, 50 p.
- Pelleg, D., and Moore, A., 2000, X-means: Extending k-means with efficient estimation of the number of clusters: in *Proceedings of the Seventeenth International Conference on Machine Learning*, v. 1, p. 727-734.
- Peltier, W. R., and Tushingham, A. M., 1989, Global sea level rise and the greenhouse effect: might they be connected?: *Science*, v. 44, p. 806-810.
- Penland, S., and Ramsey, K., 1990, Sea-level rise in Louisiana and the Gulf of Mexico: 1908-1988: *Journal of Coastal Research*, v. 6, no. 2, p. 323-342.
- Pereira, P. S., Calliari, L. J., and Barletta, R. C., 2010, Heterogeneity and homogeneity of Southern Brazilian beaches: A morphodynamic and statistical approach: *Continental Shelf Research*, v. 30, no. 3-4, p. 270-280.

- Price, W. A., 1956, Hurricanes affecting the coast of Texas from Galveston to the Rio Grande: U.S. Army Corps of Engineers Beach Erosion Board, Technical Memorandum No. 78, 35 p.
- Pries, A. J., Miller, D. L., and Branch, L. C., 2008, Identification of structural and spatial features that influence storm-related dune erosion along a barrier-island ecosystem in the Gulf of Mexico: *Journal of Coastal Research*, v. 24, p. 168-175.
- Roth, David, 2010, Texas hurricane history: National Weather Service, Camp Springs, Maryland, 83 p. <http://origin.hpc.ncep.noaa.gov/research/txhur.pdf>
- Rosati, J. D., Wise, R. A., Kraus, N. C., and Larson, M., 1993, SBEACH: Numerical Model for Simulating Storm-Induced Beach Change. Report 3 User's Manual (Instruction Report No. CERC-93-2). Washington, D.C.: US Army Corps of Engineers.
- Sallenger, A. H., 2000, Storm impact scale for barrier islands: *Journal of Coastal Research*, v. 16, p. 890-895.
- Shalowitz, A. L., 1964, Shore and beach boundaries: U.S. Department of Commerce, Publication 10-1, 749 p.
- Simpson, R. H., and Riehl, H., 1981, The hurricane and its impact: Baton Rouge, Louisiana State University Press, 398 p.
- Snay, R., Cline, M., Dillinger, W., Foote, R., Hilla, R., Kass, W., Ray, J., Rohde, J., Sella, G., and Soler, S., 2007, Using global positioning system-derived crustal velocities to estimate rates of absolute sea level change from North American tide gauge records: *Journal of Geophysical Research*, v. 112, B04409, doi: 10.1029/2006JB004606, 11 p.
- Stockdon, H. F., Doran, K. S., and Sallenger, A. H., 2009, Extraction of lidar-based dune-crest elevations for use in examining the vulnerability of beaches to inundation during hurricanes: *Journal of Coastal Research Special Issue No. 53*, p. 59-65.
- Swanson, R. L., and Thurlow, C. I., 1973, Recent subsidence rates along the Texas and Louisiana coast as determined from tide measurements: *Journal of Geophysical Research*, v. 78, p. 2665-2671.
- Texas General Land Office, 2011, A report to the 82nd Legislature Coastal Erosion Planning & Response Act: Austin, TX: Texas General Land Office, 180 pp.
- Thieler, E. R., Himmelstoss, E. A., Zichichi, J. L., and Ergul, Ayhan, 2009, Digital Shoreline Analysis System (DSAS) version 4.0 — An ArcGIS extension for calculating shoreline change: U.S. Geological Survey Open-File Report 2008-1278.
- Wilks, D. S., 2006, *Statistical Methods in the Atmospheric Sciences* (2nd ed.): Boston, MA: Academic Press.
- Williams, D. D., Kraus, N. C., Kelly, F. J., Smith, A. N., and Anderson, C. M., 2005, Baseline and construction monitoring of Packery Channel, Corpus Christi, Texas: In 2005 Proceedings National Conference on Beach Preservation Technology, Florida Shore and Beach Preservation Association, <http://www.fsbpa.com/publications.html>.

Page intentionally blank

APPENDIX A: ELEVATION-THRESHOLD AREAS

The following tables contain the total area (in hectares, ha) and area normalized by shoreline length (in ha/km) within each county that is above threshold elevations of 2 through 9 m NAVD88 within the lidar swath width flown in April 2010, April 2011, and September 2012. Also listed is the approximate shoreline length within each county and the total lidar area flown in each county. Data for Chambers County are included with Jefferson County.

April 2010 Airborne Lidar Survey (Total Area, ha)

County	Shore-line length (km)	Total survey area	Area > 2 m	Area > 3 m	Area > 4 m	Area > 5 m	Area > 6 m	Area > 7 m	Area > 8 m	Area > 9 m
Jefferson	54.9	4406.8	24.9	2.8	0.3	0.0	0.0	0.0	0.0	0.0
Galveston	88.3	7607.2	1287.3	412.2	307.4	203.4	154.5	129.2	105.0	0.0
Brazoria	46.2	4099.4	172.4	105.2	79.8	67.8	55.5	30.0	12.8	0.0
Matagorda	97.7	6936.7	459.2	90.5	35.7	12.9	6.0	0.0	0.0	0.0
Calhoun	49.0	2787.9	367.7	62.9	10.9	1.8	0.2	0.0	0.0	0.0
Aransas	37.5	2080.8	593.2	229.9	78.6	27.4	9.2	2.7	0.7	0.0
Nueces	32.1	2366.8	637.0	335.8	171.1	86.1	45.8	27.8	19.7	15.3
Kleberg	44.5	3106.7	1096.3	564.5	308.3	160.0	76.4	35.0	16.2	7.5
Kenedy	70.3	5103.5	1317.9	800.7	499.9	277.7	144.8	76.9	41.6	21.6
Willacy	29.1	2487.5	345.3	198.9	119.7	64.7	30.0	12.8	5.5	2.1
Cameron	47.0	3780.6	732.3	396.9	224.0	136.8	88.8	60.2	43.7	32.3

April 2010 Airborne Lidar Survey (Area Divided by Shoreline Length, ha/km)

County	Shore-line length (km)	Total survey area	Area > 2 m	Area > 3 m	Area > 4 m	Area > 5 m	Area > 6 m	Area > 7 m	Area > 8 m	Area > 9 m
Jefferson	54.9	4406.8	0.5	0.1	0.0	0.0	0.0	0.0	0.0	0.0
Galveston	88.3	7607.2	14.6	4.7	3.5	2.3	1.8	1.5	1.2	0.0
Brazoria	46.2	4099.4	3.7	2.3	1.7	1.5	1.2	0.6	0.3	0.0
Matagorda	97.7	6936.7	4.7	0.9	0.4	0.1	0.1	0.0	0.0	0.0
Calhoun	49.0	2787.9	7.5	1.3	0.2	0.0	0.0	0.0	0.0	0.0
Aransas	37.5	2080.8	15.8	6.1	2.1	0.7	0.2	0.1	0.0	0.0
Nueces	32.1	2366.8	19.8	10.5	5.3	2.7	1.4	0.9	0.6	0.5
Kleberg	44.5	3106.7	24.6	12.7	6.9	3.6	1.7	0.8	0.4	0.2
Kenedy	70.3	5103.5	18.7	11.4	7.1	4.0	2.1	1.1	0.6	0.3
Willacy	29.1	2487.5	11.9	6.8	4.1	2.2	1.0	0.4	0.2	0.1
Cameron	47.0	3780.6	15.6	8.4	4.8	2.9	1.9	1.3	0.9	0.7

April 2011 Airborne Lidar Survey (Total Area)

County	Shore-line length (km)	Total survey area	Area > 2 m	Area > 3 m	Area > 4 m	Area > 5 m	Area > 6 m	Area > 7 m	Area > 8 m	Area > 9 m
Jefferson	54.9	4576.2	37.6	5.0	0.6	0.0	0.0	0.0	0.0	0.0
Galveston	88.3	7259.3	1682.4	510.6	373.5	259.4	199.5	164.1	0.0	0.0
Brazoria	46.2	3091.0	212.2	116.0	89.1	76.7	62.0	35.2	0.0	0.0
Matagorda	97.7	4675.2	450.3	85.9	32.9	9.3	3.6	0.0	0.0	0.0
Calhoun	49.0	3794.5	489.9	81.9	13.7	2.3	0.3	0.0	0.0	0.0
Aransas	37.5	2766.7	697.4	252.3	84.6	29.4	9.8	3.1	1.0	0.5
Nueces	32.1	2310.1	594.4	324.4	165.9	81.9	42.1	24.4	16.5	12.7
Kleberg	44.5	2700.3	936.3	530.2	300.2	157.0	74.6	33.6	15.2	7.0
Kenedy	70.3	4271.2	1521.5	898.6	563.8	327.6	174.2	92.9	51.3	27.7
Willacy	29.1	1887.1	334.1	184.4	114.8	65.4	32.6	14.4	6.1	2.3
Cameron	47.0	3515.1	750.1	404.7	224.9	134.2	85.3	56.6	40.1	29.6

April 2011 Airborne Lidar Survey (Area Divided by Shoreline Length, ha/km)

County	Shore-line length (km)	Total survey area	Area > 2 m	Area > 3 m	Area > 4 m	Area > 5 m	Area > 6 m	Area > 7 m	Area > 8 m	Area > 9 m
Jefferson	54.9	4576.2	0.7	0.1	0.0	0.0	0.0	0.0	0.0	0.0
Galveston	88.3	7259.3	19.1	5.8	4.2	2.9	2.3	1.9	0.0	0.0
Brazoria	46.2	3091.0	4.6	2.5	1.9	1.7	1.3	0.8	0.0	0.0
Matagorda	97.7	4675.2	4.6	0.9	0.3	0.1	0.0	0.0	0.0	0.0
Calhoun	49.0	3794.5	10.0	1.7	0.3	0.0	0.0	0.0	0.0	0.0
Aransas	37.5	2766.7	18.6	6.7	2.3	0.8	0.3	0.1	0.0	0.0
Nueces	32.1	2310.1	18.5	10.1	5.2	2.6	1.3	0.8	0.5	0.4
Kleberg	44.5	2700.3	21.0	11.9	6.7	3.5	1.7	0.8	0.3	0.2
Kenedy	70.3	4271.2	21.6	12.8	8.0	4.7	2.5	1.3	0.7	0.4
Willacy	29.1	1887.1	11.5	6.3	3.9	2.2	1.1	0.5	0.2	0.1
Cameron	47.0	3515.1	16.0	8.6	4.8	2.9	1.8	1.2	0.9	0.6

February 2012 Airborne Lidar Survey (Total Area, ha)

County	Shore-line length (km)	Total survey area	Area > 2 m	Area > 3 m	Area > 4 m	Area > 5 m	Area > 6 m	Area > 7 m	Area > 8 m	Area > 9 m
Jefferson	54.9	3083.2	30.1	2.6	0.2	0.0	0.0	0.0	0.0	0.0
Galveston	88.3	5641.9	1266.9	418.1	307.6	207.4	158.0	131.6	0.0	0.0
Brazoria	46.2	2410.9	156.6	75.3	58.3	52.2	41.2	20.2	0.0	0.0
Matagorda	97.7	5960.1	471.3	95.4	34.2	9.1	4.1	2.9	0.0	0.0
Calhoun	49.0	2871.4	374.2	60.3	9.9	1.4	0.2	0.0	0.0	0.0
Aransas	37.5	2128.2	588.7	218.9	73.7	25.6	8.4	2.5	0.6	0.0
Nueces	32.1	1861.4	551.6	305.7	156.2	75.5	37.3	20.6	13.9	10.7
Kleberg	44.5	2595.2	944.2	531.3	300.0	155.9	73.7	32.7	14.4	6.4
Kenedy	70.3	3810.5	1211.9	757.2	475.5	267.4	139.0	73.3	40.2	21.2
Willacy	29.1	1678.9	322.4	185.9	115.2	64.1	31.2	14.2	0.0	0.0
Cameron	47.0	2931.0	725.3	395.4	218.0	128.1	79.9	52.3	36.4	26.1

February 2012 Airborne Lidar Survey (Area Divided by Shoreline Length, ha/km)

County	Shore-line length (km)	Total survey area	Area > 2 m	Area > 3 m	Area > 4 m	Area > 5 m	Area > 6 m	Area > 7 m	Area > 8 m	Area > 9 m
Jefferson	54.9	3083.2	0.5	0.0	0.0	0.0	0.0	0.0	0.0	0.0
Galveston	88.3	5641.9	14.3	4.7	3.5	2.3	1.8	1.5	0.0	0.0
Brazoria	46.2	2410.9	3.4	1.6	1.3	1.1	0.9	0.4	0.0	0.0
Matagorda	97.7	5960.1	4.8	1.0	0.4	0.1	0.0	0.0	0.0	0.0
Calhoun	49.0	2871.4	7.6	1.2	0.2	0.0	0.0	0.0	0.0	0.0
Aransas	37.5	2128.2	15.7	5.8	2.0	0.7	0.2	0.1	0.0	0.0
Nueces	32.1	1861.4	17.2	9.5	4.9	2.4	1.2	0.6	0.4	0.3
Kleberg	44.5	2595.2	21.2	11.9	6.7	3.5	1.7	0.7	0.3	0.1
Kenedy	70.3	3810.5	17.2	10.8	6.8	3.8	2.0	1.0	0.6	0.3
Willacy	29.1	1678.9	11.1	6.4	4.0	2.2	1.1	0.5	0.0	0.0
Cameron	47.0	2931.0	15.4	8.4	4.6	2.7	1.7	1.1	0.8	0.6

APPENDIX B: SBEACH MODELING

SBEACH is a two-dimensional empirical model designed to predict short-term beach and dune erosion resulting from storm events (Rosati and others, 1993). SBEACH uses cross-shore beach and dune profiles which are subjected to storm conditions defined by the user to produce a post-storm cross-shore profile. The model outputs intermediate time-step and final simulated profiles along with other parameters such as maximum water elevation plus wave setup during the simulation and profile volume change (Rosati and others, 1993). The main model inputs are initial cross-shore topographic profiles (or reaches), empirical beach and sediment transport parameters, and storm characteristics. Initial profiles and storm characteristics can be derived from actual field measurements or synthetically created; whereas sediment transport parameters are derived from calibration of the model if actual pre- and post-storm data are available.

SBEACH Calibration

The SBEACH model was calibrated at HRI with beach profiles and storm data for Mustang and North Padre Island acquired for Hurricane Ike in September 2008. Even though Hurricane Ike did not make a direct hit on the study area, it still impacted local dunes and beaches with elevated water levels and increased wave energy. Hurricane Ike made landfall on the north end of Galveston Island on September 13 (Berg, 2009). Pre- and post-storm profiles for the study area were provided by the Conrad Blucher Institute's Packery Channel Monitoring Project (PCMP). Profiles were collected on September 5 and 23, 2008 about 8 km north and 5 km south of Packery Channel. These profiles include topographic and bathymetric measurements. Six of these profiles were selected for calibration purposes.

Storm water levels were determined from primary water level measurements at the Bob Hall Pier tide gauge every six minutes from September 10 to 15. Local significant wave heights and period time series at a depth of 8.2 m were provided by Andrew Kennedy from the University of Notre Dame. Kennedy's group developed both wave heights and periods from a tightly-coupled, depth-

averaged, SWAN+ADCIRC wave and circulation model using buoy measurements deployed during Hurricane Ike along the Texas coast (Bender and others, 2010).

Initial beach and sediment transport parameters used in the calibration process were taken from previous technical reports that used SBEACH to model beach and dune storm response in South Padre Island and Galveston Island, Texas (King, 2007; Texas General Land Office, 2011). A sensitivity analysis was conducted, and the chosen combination of parameters had the smallest RMS error between the simulated and measured post-storm profiles. The resulting calibration parameters are close in range to the parameters from the King (2007) and Texas General Land Office (2011) studies.

SBEACH Modeling

HRI researchers divided the Texas coast into three sections to use model parameters that would be the closest to local conditions. From High Island to Matagorda, the following values were used: landward surf zone depth 0.5 m, effective grain size 0.14 mm, maximum slope prior avalanching 30° , transport rate coefficient $2.25 \times 10^{-6} \text{ m}^4/\text{N}$, overwash transport parameter 0.005, coefficient for slope-dependent term $0.002 \text{ m}^2/\text{s}$, transport rate decay coefficient multiplier 0.5, and water temperature 29.5° C (Texas General Land Office, 2011). From Matagorda to Yarborough Pass, these same values were used except for an effective grain size of 0.15 mm (Texas General Land Office, 2011; Williams and others, 2005). From Yarborough Pass to South Padre Island, most of the values remained the same except for an effective grain size of 0.18 mm and a transport rate coefficient of $2.5 \times 10^{-6} \text{ m}^4/\text{N}$ (Texas General Land Office, 2011).

Representative Profiles

HRI researchers divided the Texas coast into 15 regions at inlets or passes. 10,177 cross-shore profiles were cast every 50 m alongshore, starting at the local mean sea-level contour to the landward boundary of the foredune complex. Elevation points were extracted every 2 m along each

profile from a filtered DEM for 2010 and 2012 derived from lidar data collected by the Bureau for this project.

Cluster analysis was used as a data reduction method to select representative profiles for the study area. Cluster analysis sorts data into groups based on the degree of similarity and difference among observations (Wilks, 2006). Pereira and others (2010) applied cluster analysis along with multidimensional scaling to a data set of profile morphometric parameters to group beaches with similar morphodynamic characteristics at a regional scale. In this study, we selected a K-means clustering method using as input a data matrix with cross-shore elevation data (columns) from casted profiles (rows). Profiles that intersected piers, jetties, and seawalls were not included. To find the optimal number of clusters (k) for each region, we used an algorithm proposed by Pelleg and Moore (2000) based on the Bayesian Information Criterion. The mean of each of the k clusters is then considered a representative profile. All representative profiles were assigned the same mean bathymetry section derived from the 2008 PCMP pre-Ike survey data to focus on the comparative response of the subaerial part of the profiles along the entire Texas coast.

Synthetic Storms

Storm conditions used in SBEACH simulations were synthetically created at HRI using Hurricane Ike as the reference. Eight different storms representing different return periods were created by scaling tide gauge and buoy measurements during Ike for primary water level, wave height, and peak wave period at a 6-minute time step during Ike. Measurements for the reference conditions were made by instruments located in the right-front quadrant area of the storm from September 11 to 14, 2008. Primary water level measurements were collected by NOAA's tide gauge 87770570 in Sabine Pass; wave height measurements were collected by Kennedy Station Z buoy close to Sabine Pass; and peak wave periods were taken from a post-Ike STWAVE simulation at Kennedy Station Z (Bender and others, 2010). Eight reference time series curves were derived from the actual measurements, making each point a percentage of the maximum measured value. The percentage curves were then multiplied by maximum values for each storm

return period and smoothed using a multiple-term Gaussian algorithm from MATLAB’s curve fitting toolbox. All maximum synthetic values for water level, wave height, and wave period curves were taken from the Economic and Natural Resource Benefits section of the most recent Coastal Erosion Planning and Response Act (CEPRA) report (Texas General Land Office, 2011); except for the 200-year storm, which was calculated as an extrapolation from the values in the CEPRA report.

The eight synthetic storms with return periods of 1, 2, 5, 10, 20, 50, 100, and 200 years were used to represent a wide range of conditions. All synthetic storms have duration of 72 hours. Table B1 lists the return period, maximum surge (water level) value, maximum wave height, and peak wave period for each of the eight synthetic storms.

Level of Protection Provided by Dune and Beach Environments

The theoretical level of storm protection was determined at HRI using a quantitative assessment of the beach/dune profile changes after simulating the set of synthetic storms. The goal was to identify the storm level at which dune/beach profiles are overwashed. Using SBEACH simulation outputs, the focus was on the maximum water depth value reached during the simu-

Table B1. Synthetic storms parameters (from HRI).

Storm	Return period	Max. surge (m)	Max. wave height (m)	Peak period (sec)
1	1-year	0.64	3.53	10.10
2	2-year	0.73	4.05	10.70
3	5-year	0.97	4.81	11.00
4	10-year	1.34	5.27	11.80
5	20-year	1.91	5.85	12.30
6	50-year	3.00	6.55	12.90
7	100-year	3.66	7.07	13.40
8	200-year	5.02	7.60	14.04

lation along the profile. A dune/beach profile is considered to have been overwashed, and thus not offering protection, if the maximum water depth hydrograph indicates that water was present landward of mean beach/foredune complex width for the representative profile during the simulation. Profiles that were not modeled were assigned a level of protection according to their geomorphology, or engineering design if they intersected human-made structures. Profiles in Jefferson County and Surfside Beach were assigned the lowest level of protection due to their narrow beach and low/absent dunes. Profiles in front the Galveston and North Padre Island seawalls were assigned a 100-yr protection level consistent with their design base elevations (Galveston: 5.4 m, NPI: 3.5 m). The level of protection provided by a beach/dune profile is expressed in terms relative to other profiles along the Texas coast.

APPENDIX C: DATA VOLUME CONTENTS

The hard drive that accompanies this report contains data acquisition reports, data deliverable reports, a presentation, and lidar and geographic information system (ESRI ArcGIS 10.1 compatible) files from the April 2010, April 2011, and February 2012 airborne lidar surveys of the Texas Gulf coast conducted by the Bureau of Economic Geology on behalf of the Texas General Land Office. The lidar and GIS products are final deliverables for the project titled “Shoreline Change and Beach/Dune Morphodynamics Along the Gulf Coast,” GLO contract number 09-242-000-3789.

All spatial data are in the UTM projection, North American Datum 1983 (NAD83), zone 14 or 15 north. Elevation and coordinate units are in meters. Elevation data are relative to the North American Vertical Datum 1988 (NAVD88).

A folder-by-folder description of the contents of the disk follows.

DuneBoundary: contains ArcGIS-compatible shapefiles depicting the landward dune boundary for 2010, 2011, and 2012.

LIDAR: contains April 2010, April 2011, and February 2012 all-point LAS files, ASCII digital elevation models, and associated metadata separated by UTM zone. Due to the size of the lidar data deliverables LAS files are presented as quadrangle files, DEMs are presented as quarter-quadrangle files.

Presentations: contains a pdf of a project-related presentation given by Dr. Jeff Paine at the 2013 American Shore and Beach Preservation Association National Coastal Conference in South Padre Island, Texas on October 24, 2013.

PVL: contains ArcGIS-compatible shapefiles depicting the 1.2 m msl potential vegetation line position for 2010, 2011, and 2012.

Reports: contains three Bureau of Economic Geology reports summarizing airborne data acquisition activities for April 2010, April 2011, and February 2012. This folder also contains three Bureau of Economic Geology reports summarizing the GIS products deliverables derived from the annual surveys. The folder also contains high- and low-resolution versions of the final project report (this document).

ShorelineChange: contains ArcGIS-compatible shapefiles depicting short-term shoreline change for the time intervals 2010-2011, 2011-2012, and 2010-2012.

Shorelines: contains ArcGIS-compatible shapefiles depicting the 0.6 m msl shoreline position for 2010, 2011, and 2012.

SSI: contains ArcGIS-compatible shapefiles depicting the Storm Susceptibility Index for the Texas Gulf coast.